

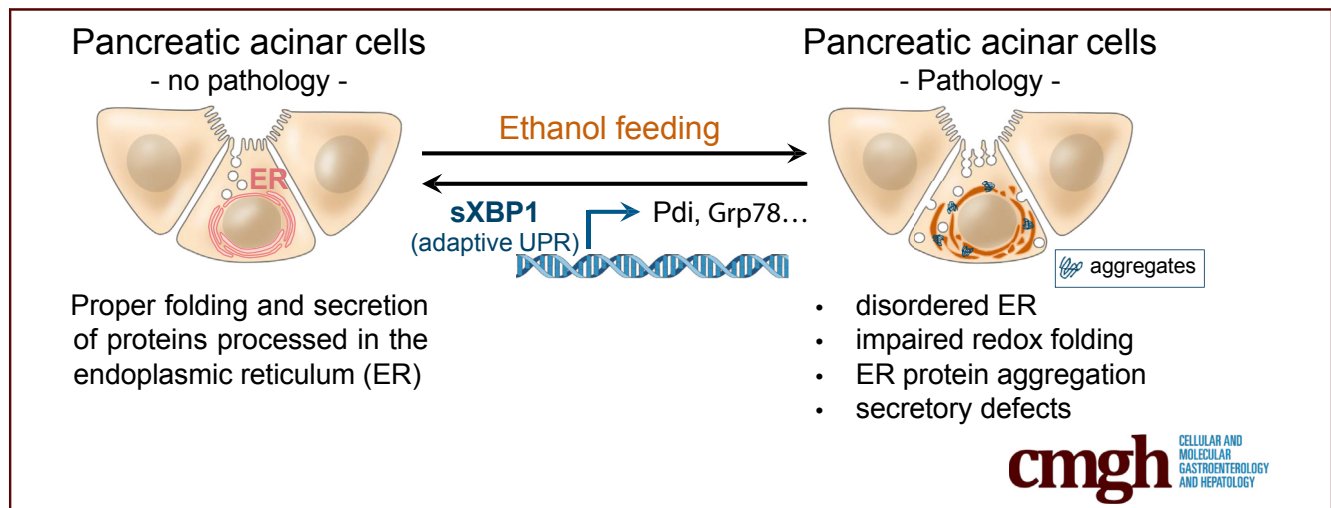
ORIGINAL RESEARCH

Ethanol Induced Disordering of Pancreatic Acinar Cell Endoplasmic Reticulum: An ER Stress/Defective Unfolded Protein Response Model



Richard T. Waldron,^{1,2} Hsin-Yuan Su,¹ Honit Piplani,¹ Joseph Capri,³ Whitaker Cohn,³ Julian P. Whitelegge,³ Kym F. Faull,³ Sugunadevi Sakkiah,¹ Ravinder Abrol,¹ Wei Yang,¹ Bo Zhou,¹ Michael R. Freeman,^{1,2} Stephen J. Pandol,^{1,2} and Aurelia Lugea^{1,2}

¹Department of Medicine, Cedars Sinai Medical Center, Los Angeles, California; ²Department of Medicine, or ³Psychiatry and Biobehavioral Sciences, University of California Los Angeles David Geffen School of Medicine, Los Angeles, California



SUMMARY

Heavy alcohol consumption is associated with pancreas damage, but light drinking shows the opposite effects, reinforcing proteostasis through the unfolded protein response orchestrated by X-box binding protein 1. Here, ethanol-induced changes in endoplasmic reticulum protein redox and structure/function emerge from an unfolded protein response-deficient genetic model.

BACKGROUND & AIMS: Heavy alcohol drinking is associated with pancreatitis, whereas moderate intake lowers the risk. Mice fed ethanol long term show no pancreas damage unless adaptive/protective responses mediating proteostasis are disrupted. Pancreatic acini synthesize digestive enzymes (largely serine hydrolases) in the endoplasmic reticulum (ER), where perturbations (eg, alcohol consumption) activate adaptive unfolded protein responses orchestrated by spliced X-box binding protein 1 (XBP1). Here, we examined ethanol-induced early structural changes in pancreatic ER proteins.

METHODS: Wild-type and *Xbp1*^{+/-} mice were fed control and ethanol diets, then tissues were homogenized and fractionated. ER proteins were labeled with a cysteine-reactive probe, isotope-coded affinity tag to obtain a novel pancreatic redox ER proteome. Specific labeling of active serine hydrolases in ER with fluorophosphonate desthiobiotin also was characterized proteomically. Protein structural perturbation by redox changes was evaluated further in molecular dynamic simulations.

RESULTS: Ethanol feeding and *Xbp1* genetic inhibition altered ER redox balance and destabilized key proteins. Proteomic data and molecular dynamic simulations of Carboxyl ester lipase (Cel), a unique serine hydrolase active within ER, showed an uncoupled disulfide bond involving Cel Cys266, Cel dimerization, ER retention, and complex formation in ethanol-fed, XBP1-deficient mice.

CONCLUSIONS: Results documented in ethanol-fed mice lacking sufficient spliced XBP1 illustrate consequences of ER stress extended by preventing unfolded protein response from fully restoring pancreatic acinar cell proteostasis during ethanol-induced redox challenge. In this model, orderly protein folding and transport to the secretory pathway were disrupted,

and abundant molecules including Cel with perturbed structures were retained in ER, promoting ER stress-related pancreas pathology. (*Cell Mol Gastroenterol Hepatol* 2018;5:479–497; <https://doi.org/10.1016/j.jcmgh.2018.01.001>)

Keywords: Alcohol Pancreatitis; Carboxyl Ester Lipase; Disulfide Bond; Unfolded Protein Response.

Although heavy drinking is a risk factor for both acute and chronic pancreatitis,¹ only a small minority of alcohol abusers acquire pancreatic diseases.² Pancreatitis is initiated in the pancreatic acinar cell upon acinar cell dysfunction.³ The acinar cells are specialized secretory cells with a prominent role as biosynthetic factories producing and secreting digestive enzymes. An extensive ribosome-studded endoplasmic reticulum (ER) network in these cells enables high rates of enzyme production.⁴ Several studies have indicated that disorders in ER function are associated with acute and chronic pancreatitis,^{5–10} but the precise alterations in ER components and ER protein processing during pancreatitis are poorly defined.

Protein folding in the acinar cell ER requires balanced redox conditions.¹¹ We previously found adverse effects of chronic ethanol feeding in pancreas ER, such as an increased oxidized-to-reduced-glutathione ratio.^{12,13} This perturbs protein folding and induces an unfolded protein response (UPR) involving up-regulation of the UPR transcription factor, spliced X box-binding protein 1 (sXBP1) that limits ethanol-mediated damage.^{10,12} In this respect, genetic deletion of XBP1 in mice prevented increases in sXBP1, associated with severe ER stress, disordered autophagy, decreased secretion of digestive enzymes from acinar cells, acinar cell death, and pancreas damage.^{12,14} More recently, we also found that cigarette smoke extracts reduced sXBP1 levels, and increased ethanol-induced ER stress and cell death in acinar cells.¹⁰ Moreover, rats exposed to cigarette smoke showed lower pancreatic sXBP1 levels and more severe alcoholic pancreatitis than control animals.¹⁰ These studies led us to propose that sXBP1 plays an essential role to prevent ethanol-induced ER dysfunction. Here, our goal was to identify novel ethanol feeding-induced changes in protein processing in the ER that precede and sensitize the pancreas to frank pathologic damage.

Because ethanol altered ER redox, and XBP1 genetic deficiency (in *Xbp1*^{+/-} mice) increased damage in the context of ethanol feeding, we focused on the role of ethanol-induced protein oxidation in pancreatic pathology. We hypothesized that the ethanol feeding-induced increase in sXBP1 in the acinar cell supports normal protein processing and trafficking in wild-type mice by correcting redox-induced changes in ER proteins. We further predicted that ethanol would lead to accumulation of redox-driven misfolding or other alterations in ER proteins in *Xbp1*^{+/-} mice (with a deficient UPR). We used liquid chromatography–tandem mass spectrometry (LC-MS/MS) to characterize effects of ethanol feeding and XBP1 deficiency on pancreatic ER proteins, and OXICAT^{15,16} to quantify protein disulfides after reaction of cysteine

sulfhydryls with isotope-coded affinity tags (ICAT). To complement this approach, we also searched for peptides with cysteines modified by other biochemical residues.

Many abundant secretory proteins synthesized in the ER of the acinar cell belong to the serine hydrolase enzyme family.¹⁷ Although most serine hydrolases (eg, trypsin) are produced as inactive proenzymes, aberrant activation within the cell has been mechanistically linked to pancreas pathology. Altered cysteine oxidation and disulfide bond formation might overtly change serine hydrolase activity by altering protein structure. We therefore also investigated the activity of serine hydrolases in the ER fraction to show their potential to act as causal links between ethanol feeding, deficient UPR, and pancreatic pathology.

Materials and Methods


Experimental Animal Model of Impaired Oxidative Refolding in Pancreas

XBP1-deficient (*Xbp1*^{+/-}) and wild-type ([WT] *Xbp1*^{+/+}) mice were used for the study. Detailed information about *Xbp1*^{+/-} mouse genotype and phenotype, diet composition, and intragastric feeding procedure is provided later. Pancreas and pancreatic acinar cell pathology in this model was reported previously.^{12,14}

XBP1-Deficient Mice

We used mice with a null mutation in 1 *Xbp1* allele (*Xbp1*^{+/-}) and littermate WT controls (*Xbp1*^{+/+}, BALB/c background). *Xbp1*^{+/-} mice were generated by Ozcan et al,¹⁸ and have been described previously.¹² We used *Xbp1* heterozygous mice because complete *Xbp1* deletion results in embryonic lethality, and pancreas-specific deletion results in rapid, extensive acinar cell death.¹⁹ In regular housing conditions and compared with WT mice, protein levels of sXBP1 and unspliced (u) XBP1 in pancreas are reduced ~40% and ~30%, respectively, in *Xbp1*^{+/-} mice.¹² *Xbp1*^{+/-} mice are fertile and healthy, and grow at a rate similar than their WT littermates when maintained on standard chow diets. However, compared with WT, *Xbp1*^{+/-} mice show increased hepatic ER stress and insulin resistance when placed on a high-fat diet for 16 weeks.¹⁸ Moreover, *Xbp1*^{+/-} mice fed intragastrically with ethanol-containing diets show in pancreatic acinar cells signs of ER stress, decreased numbers of zymogen granules, increased autophagy, and 10%–15% loss of acinar cells.¹²

Abbreviations used in this paper: ATPase, adenosine triphosphatase; Cel, carboxyl ester lipase; DTT, dithiothreitol; ER, endoplasmic reticulum; ERAD, endoplasmic reticulum-associated degradation; FAEE, fatty acid ethyl esters; FP, fluorophosphonate; ICAT, isotope-coded affinity tags; LC-MS/MS, liquid chromatography–tandem mass spectrometry; MW, molecular weight; %-ox, percentage oxidized; RER, rough ER; sXBP1, spliced X box-binding protein 1; UPR, unfolded protein response; WT, wild type.

 Most current article

© 2018 The Authors. Published by Elsevier Inc. on behalf of the AGA Institute. This is an open access article under the CC BY-NC-ND license (<http://creativecommons.org/licenses/by-nc-nd/4.0/>).

2352-345X

<https://doi.org/10.1016/j.jcmgh.2018.01.001>

Intragastric Ethanol Feeding in Mice

Chronic ethanol feeding was performed at the Animal Core of the Southern California Research Center for Alcoholic Liver and Pancreatic Diseases and Cirrhosis. Ethanol and control diets were provided using the Tsukamoto-French intragastric ethanol infusion model as previously described.²⁰ This model was selected because it allows accurate control of nutrient intake and alcohol consumption patterns. In this model, mice are pair-fed isocaloric amounts of liquid diet containing ethanol (ethanol diet) or dextrose as a substitute for ethanol (control diet) by a continuous intragastric infusion method. Control and ethanol diets had the same protein (lactoalbumin hydrolysate) and fat (corn oil) composition and only differed in the content of ethanol and dextrose. The diets also contained citric acid, choline chloride, and a mix of salts, vitamins, and minerals at concentrations recommended by the Committee on Animal Nutrition of the National Research Council (Dyets, Inc, Bethlehem, PA). Nutrients were purchased from Invitrogen Corporation (Carlsbad, CA), Sigma Chemical Co (St. Louis, MO), and Dyets, Inc. All experimental procedures were approved by the Institutional Animal Care and Use Committees of Cedars-Sinai Medical Center and the University of Southern California.

For this study, we used a total of 14 male WT mice and 13 male *Xbp1*^{+/-} mice. Mice were housed under controlled conditions of temperature, humidity, and a 12-hour light/dark cycle with free access to water and rodent chow diet before ethanol feeding. At the age of 12–14 weeks, mice underwent surgery aseptically under general anesthesia (ketamine and xylazine) for implantation of long-term gastrostomy catheters. After a 4- to 6-day acclimatization period on chow diet, mice were distributed randomly into the control or the ethanol diet group, and continuous ethanol infusion was initiated in the ethanol group at the initial ethanol dose of 22.7 g/kg/day, and incrementally increased to 30–33 g/kg/day over a 4-week period. Control-fed animals were infused simultaneously with isocaloric amounts of dextrose. At the initial ethanol dose, total calories derived from the diet and ethanol was set at 568 cal/kg/day, and the caloric percentages of ethanol, dextrose, protein, and fat were 29%, 11%, 25%, and 35%, respectively. The highest ethanol dose at the end of 6 weeks accounted for approximately 34%–37% of calories.

After 6 weeks on diets, animals were killed and tissue samples were taken for analysis. Blood ethanol levels at death, determined by an Analox GM7 analyzer (Analox Instruments, Atlanta, GA), were comparable between WT (means \pm SEM, 220 mg/dL \pm 5 mg/dL) and *Xbp1*^{+/-} mice (means \pm SEM, 280 mg/dL \pm 10 mg/dL), suggesting that XBP1 deficiency does not alter ethanol metabolism.

Body weight was monitored through the ethanol feeding period. Mice in the 4 treatment groups had similar body weight at the beginning of the diets: WT control diet, 25.7 g \pm 0.4 g; *Xbp1*^{+/-} control diet, 25.6 g \pm 1.6 g; WT ethanol diet, 25.0 g \pm 0.8 g; *Xbp1*^{+/-} ethanol diet, 25.4 g \pm 1.2 g (means \pm SEM, n = 5–8). After 6 weeks on diets, body weight gain was significantly lower in ethanol-fed *Xbp1*^{+/-} mice compared with ethanol-fed WT mice. Body weight gain,

expressed as a percentage of body weight at death vs initial body weight (means \pm SEM, n), was as follows: WT control diet, 116.9 \pm 2.3 (n = 7); *Xbp1*^{+/-} control diet, 113.1 \pm 0.6 (n = 5); WT ethanol diet, 105.4 \pm 2.6 (n = 7); *Xbp1*^{+/-} ethanol diet, 96.4 \pm 2.1 (n = 8) (*P* = .029 vs WT ethanol diet, 2-way analysis of variance and Tukey post-test).

Isolation of Endoplasmic Reticulum Fractions

Mice were euthanized by CO₂ asphyxiation, and pancreas tissue was immediately isolated and homogenized in 1.8 mL buffer (buffer A) comprising 5 mmol/L (2-(N-Morpholino) ethanesulfonic acid, 5 mmol/L MgCl₂, pH 7.0, with 1 mmol/L dithiothreitol (DTT) using a rotary homogenizer with a polytetrafluoroethylene (PTFE) pestle, for 6 strokes at 80% of full speed. This low amount of DTT was included in buffer A to prevent widespread oxygenation and cross-linking of mostly extracellular proteins. Its reducing capacity should be consumed before complete cell lysis and separation of membrane fractions. The homogenate was diluted to 5 mL with buffer A (without further DTT) and further homogenized in a 7-mL Dounce (Wheaton, Millville, NJ) glass homogenizer. The homogenate was brought to 0.25 mol/L sucrose, and sequentially spun at 150 \times g for 10 minutes, 1300 \times g for 10 minutes, and 10,000 \times g for 15 minutes, with the supernatant carried forward. The rough ER fraction was pelleted from this supernatant by centrifuging at 85,000 \times g for 30 minutes. Centrifugation was performed in thick-walled Beckman (Beckman Coulter, Brea, CA) tubes in a TY-65 rotor (Beckman). Pellets were resuspended in Buffer A (no DTT) containing 0.25 mol/L sucrose, and snap frozen in N₂(l) for later analysis. Protein concentration in the RER samples was obtained using the Pierce BCA (Thermo Fisher Scientific, Asheville, NC) protein assay system.

Western Blot and ER Protein Reaction With Biotinylated Serine Hydrolase Activity Probe

Pancreatic ER fractions as well as total tissue lysates were examined by Western blot as follows: ER fractions (10–20 μ g) were separated on Invitrogen Tris-glycine sodium dodecyl sulfate–polyacrylamide gel electrophoresis 4%–20% gradient gels, transferred to nitrocellulose membranes using Bio-Rad (Hercules, CA) TransBlot Turbo rapid transfer system (15 minutes at a constant current of 1.25 A per minigel), and blocked with 5% bovine serum albumin in Tris-buffered saline buffer with 0.075% Tween 20. Subsequent incubations and washes were performed in Tris-buffered saline with 0.075% Tween 20. Primary antibodies used against lipase, carboxyl ester lipase (Cel) (sc-34878), signal recognition particle 72 were from Santa Cruz Biotechnologies (Santa Cruz, CA). Extracellular signal-regulated kinase 1/2 antibody was from Cellular Signaling Technologies (Beverly, MA). ActivX Desthiobiotin-FP Serine Hydrolase Probe and streptavidin–horseradish peroxidase were from Thermo Fisher Scientific. ER fractions (50 μ g) were incubated with probe (2 μ g/mL) in 10 mmol/L Tris-HCl, pH 7.4 for 20 minutes at room temperature, then Triton X-100 (Bio-Rad) was added to 1% and the

clarified mixture was incubated for a further 20 minutes at room temperature. Samples then were prepared by addition of gel loading buffer and further processed for Western blot as described earlier.

Mass Spectrometric Determination of Protein and Peptide Content of Pancreas ER Fractions

In-gel digest of Coomassie-stained gels was performed to generate samples from a single gel (2–3 lanes per condition), divided into 8 molecular weight (MW) ranges between 15 and 150 kilodaltons. Proteomic analysis was performed by LC-MS/MS on an Orbitrap Elite (Thermo Fisher Scientific) mass spectrometer at the Biomarker Discovery Platform at Cedars-Sinai Medical Center. The data were processed by Mascot (Matrix Science, Boston, MA) and then by Maxquant v.1.4.0.0 (Jurgen Cox, Max Planck Institute of Biochemistry). Results obtained from WT and *Xbp1*^{+/-} mice were pooled to quantitate differences between control- and ethanol-fed mice ER fractions (and between WT and *Xbp1*^{+/-} mice) using spectral counting. Protein IDs with least 2 unique peptides and 2 or more peptide spectra matches were analyzed. Differences in spectral count across the 32 LC-MS/MS runs were normalized as described.²¹ Briefly, spectral counts were summed across each chromatogram. Values within each run were multiplied by a factor comprising the sum of spectral counts in that run divided by the sum of the maximal spectral counts in a single run. Normalized values were uploaded to Qspec Spectral Counter (www.nesvilab.org/qspec.php/)²²; output files enabled us to quantitate the proteins that increased or decreased by fold-changes. The Orbitrap Elite also was used to analyze peptide modifications in (avidin column) flow through from the ICAT experiment, and provided complementary proteomic data incorporated.

Extraction of Membrane Fractions, Labeling With ICAT Reagents, and Purification of Labeled Tryptic Peptides

RER fractions (100 μ g) were extracted by shaking for 15 minutes at 37°C in buffer comprising 100 mmol/L Tris, pH 7.0, containing 25% acetonitrile, 0.1% sodium dodecyl sulfate, and 0.05% sodium deoxycholate (Buffer B), in 1.5 mL Eppendorf (Thermo Fisher Scientific) Protein LoBind tubes flushed of air using N₂ gas. Next, 75 μ L of a 1:1 slurry of Cleanascite (Biotech Support Group, Monmouth Junction, NJ) delipidizing beads were added, and the tubes were flushed with N₂ gas and rotated end-over-end for 15 minutes at room temperature. Slurries were spun at 10,000 rpm for 5 minutes at room temperature, clarified extracts were transferred to clean tubes, and pelleted beads were discarded. Trichloroacetic acid (10% final concentration) was added and the samples were incubated on ice for 3 hours.¹⁵ Precipitated protein was recovered by centrifugation at 15,000 rpm for 15 minutes at 4°C. The supernatant was aspirated, and the pellets were redissolved in 80 μ L of Buffer B. Each sample was labeled using 1 vial of light ICAT reagent (Sciex, Inc, Foster City, CA), according to the instructions provided. The proteins then were reprecipitated with 10% trichloroacetic acid, washed twice with ice-cold acetone (600 μ L) to remove excess ICAT reagent, redissolved in 80 μ L of Sciex, Inc, denaturing

buffer containing 8 mol/L guanidine, disulfides were reduced by addition of tris(2-carboxyethyl)phosphine to 1.25 mmol/L, and heating to 80°C for 1 hour. Next, heavy ICAT labeling was achieved by combining the reagent with the sample as instructed and shaking for 1 hour at 37°C. Proteins were again precipitated using 10% TCA, washed twice with acetone, redissolved in trypsin solution, and digested overnight at 37°C. Peptides were recovered by batch chromatography on cation exchange and avidin columns (Sciex, Inc), dried in a vacuum centrifuge, redissolved in trifluoroacetic acid solution to cleave off the biotin, redried, and redissolved in 10% acetonitrile, 1% formic acid for mass spectrometric evaluation.

Mass Spectrometry of ICAT-Labeled Peptides

ICAT-labeled pancreas ER peptides eluted from avidin columns were analyzed using a Thermo LTQ Orbitrap XL mass spectrometer with an Eksigent LC. Intensities obtained from heavy and light ICAT-labeled peptides were normalized as described earlier. The percentage oxidized (%-ox) of individual peptides was calculated as the heavy intensity divided by the sum of light and heavy intensities.

Structural Modeling Computation of Carboxyl Ester Lipase

The atomic structure of mouse Cel (Uniprot Q64285; www.uniprot.org/) was built by comparative homology modeling using Discovery Studio v 3.5 (Accelrys, San Diego, CA). Two different conformations from crystal structures (Protein Data Bank ID: 1AKN and 1F6W) were used as a template to determine the 3-dimensional structure of Cel. The best monomer structures from each template (model 1 from 1akn and model 2 from 1f6w) were selected from the 10 generated models using the discrete optimized protein energy score from Discovery Studio. The Cel homodimer was generated by adopting the dimer topology from the lipase crystal structure (Protein Data Bank ID: 3DNM). Model 1 and model 2 were used as starting structures to generate Cel homodimers: model 1_dimer and model 2_dimer. Both dimer structures were relaxed by implicit solvent energy minimization using GROMACS (GROningen MACHine for Chemical Simulations, Uppsala, Sweden) 4.5.6 and the Amber (Assisted Model Building with Energy Refinement; ambermd.org) force field. Cys266 and Cys277 were both mutated to alanine (reduced) in monomer and dimer models to mimic the ethanol-induced disruption of the Cys 266–Cys277 bond (eg, by oxidation of Cys266), as suggested by our LC-MS/MS data. The WT and reduced monomer and dimer structures were relaxed in an aqueous environment by 100-ns molecular dynamics simulations in the presence and absence of 300 μ mol/L Ca²⁺. Representative structures for monomers and dimers were selected as snapshots closest to the average structure from simulation trajectories. Analysis of formation of the catalytic triad in the monomers and dimers, and interactions between the protomer units in dimers, were performed for selected representative complexes using Discovery Studio. Template 1 (from PDB ID: 1AKN) was chosen because it led to lower energy structures for Cel.

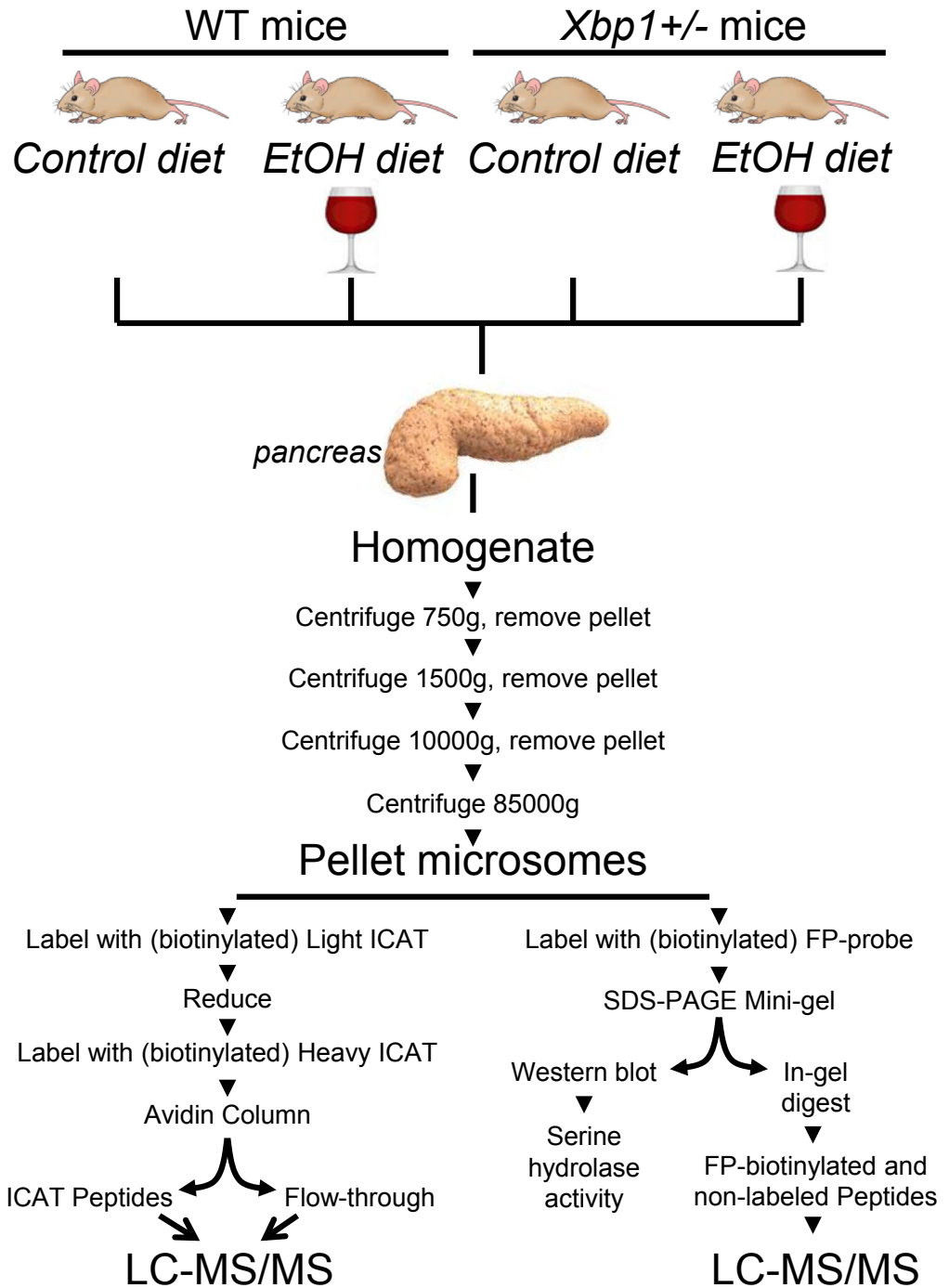


Figure 1. Study design. EtOH, ethanol diet; SDS-PAGE, sodium dodecyl sulfate–polyacrylamide gel electrophoresis.

Culture, Ethanol Treatment, and Protein Aggregation Assay of Rat AR42J Pancreatic Acinar Cells

AR42J cells (ATCC, Rockville, MD) were cultured in F-12K medium (ATCC) supplemented with 17% (vol/vol) fetal bovine serum and antibiotics/antimycotics (Omega Scientific, Tarzana, CA) at 37°C in a humidified atmosphere of 95% air and 5% CO₂ and differentiated into an acinar cell-like

phenotype by exposure to (100 nmol/L) dexamethasone for 72 hours. Medium then was replaced with F-12K containing 8.5% fetal bovine serum and cells were treated with ethanol (100 mmol/L, 459836; Sigma-Aldrich) for 48 hours. Treated plates were enclosed in a MIC-101 (Billups-Rothenberg; <http://www.brincubator.com/hypoxiachamber.htm>) hypoxia chamber together with 200 mL of ethanol (200 mmol/L) in uncovered plates to minimize ethanol evaporation. Two open

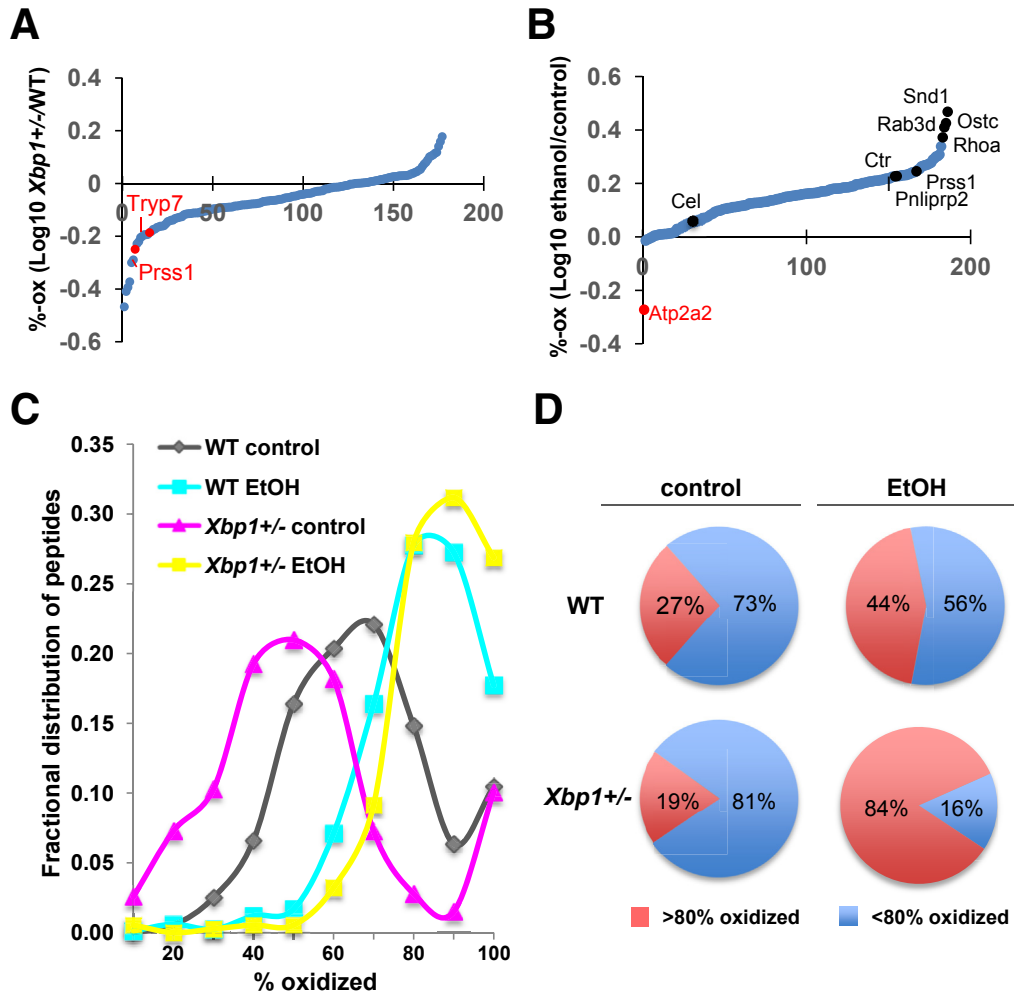


Figure 2. Comparison of %-ox proteins by mouse genotype and diet. (A) Data of %-ox proteins were compared between ER proteome samples obtained from WT and $Xbp1^{+/-}$ mice fed control or ethanol (EtOH) diet. Average ratios of $Xbp1^{+/-}$ to WT were computed and \log_{10} values were plotted vs peptide number for each peptide detected at least 3 times. (B) Comparison of %-ox data between control- and EtOH-fed ER samples. Average ratios of EtOH- to control-fed were computed and \log_{10} values plotted vs peptide number for each peptide detected at least 3 times. (C) Histograms (fractional distributions) of peptide %-ox values plotted according to treatment condition. ER peptides from control-fed $Xbp1^{+/-}$ mice (pink) are shifted toward more reducing %-ox compared with WT (grey). Peptides from EtOH-fed WT mice (green) are more oxidized, and those from $Xbp1^{+/-}$ mice (yellow) are even more severely oxidized because the initial shift toward reduced status exposes more sulfhydryls to the oxidizing conditions associated with ethanol feeding. *P* values were as follows: 1.0×10^{-37} $Xbp1^{+/-}$ control vs WT control; 2.3×10^{-62} WT EtOH vs WT control; and 1.1×10^{-6} $Xbp1^{+/-}$ EtOH vs WT EtOH. (D) Graphic illustration of the shifts in peptide redox status associated with different conditions. Average fold-changes and *P* values for individual comparisons are shown in [Supplementary Table 1](#).

chamber gas outlets (~7-mm diameter) allowed CO₂ exchange with culture medium. The chamber was placed inside a 10% CO₂ incubator to preserve medium pH. Cells from 3–4 (100-mm) dishes were combined, hypotonically lysed, and fractionated into pellets upon sequential centrifugation steps of 150, 750, 1300, 5000, 12,000, and 100,000 × *g*, using buffers containing protease inhibitors and other additives similar to the tissue fractionation steps described earlier.

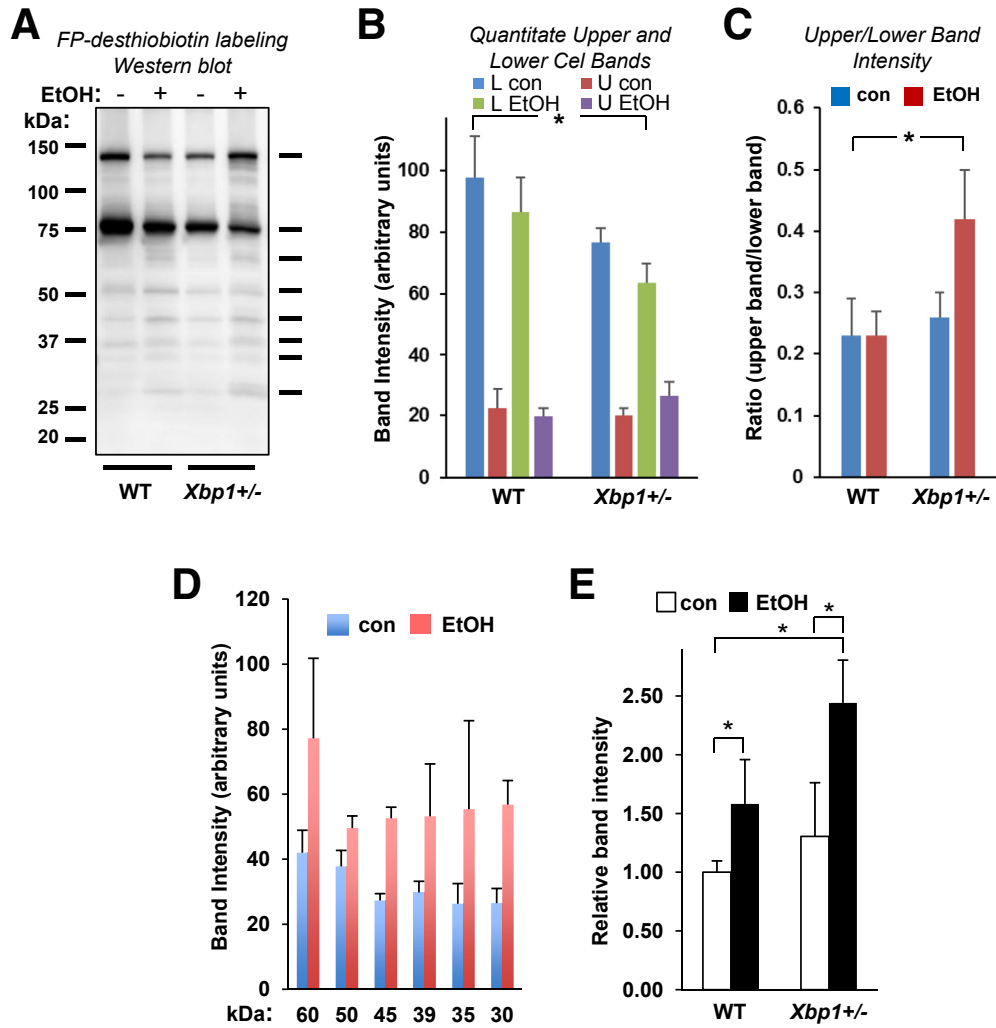
For protein aggregation assays, a Proteostat aggregates detection kit (Enzo Life Science, Farmingdale, NY) was used according to the manufacturer's instructions to visualize protein aggregates by confocal microscopy. AR42J cells were plated on glass cover slips, treated with ethanol at the

indicated concentrations, then fixed and incubated with reagents before analysis. Confocal images were acquired using a Zeiss (Carl Zeiss Microscopy, Thornwood, NY) LSM 710 confocal microscope with a 63× oil objective (numeric aperture, 1.4). Laser (diode) excitation was at 561 nm, and the emission window was at 580–690 nm.

Bioinformatics

Venny 2.1 (<http://bioinfogp.cnb.csic.es/tools/venny/index.html>) was used to create the Venn diagram shown in [Figure 7](#). DAVID (The Database for Annotation, Visualization and Integrated Discovery; <https://david.ncifcrf.gov/>)

Figure 3. Quantitative effects of ethanol and *Xbp1*^{+/-} genotype on Cel monomers and dimers. (A) Representative detection by anti-biotin Western blot of Cel monomers and dimers and minor bands in ER fractions. (B) Quantitation of individual 70-kilodalton and 140-kilodalton Cel bands. (C) Comparison of Cel dimer/monomer ratio. Bands obtained in 4 experiments as shown in panel A were quantitated by densitometry, and the ratio of the upper band/lower band was calculated and plotted as means \pm SEM, $n = 3$. (D) Densitometric quantitation of relative levels of minor individual gel bands (marked with *black bars* in panel A) from ER fractions obtained from control- and ethanol-fed mice. (E) Changes in aggregate values of 6 minor serine hydrolase bands assessed in panel D mediated by ethanol-feeding and XBP1 deficiency, calculated and plotted as means \pm SEM, $n = 3$. con, control; L, lower; U, upper.



interface^{23,24} was used to assess the gene ontology of ER proteomic data (Figures 4 and 7).

Quantitation and Statistical Analysis

The data were presented as the means \pm SEM with comparisons by the Student *t* test with unequal variance using SigmaStat 3.5 (Systat Software, San Jose, CA). *P* values $< .05$ were considered to confer statistical significance. In data compared by spectral counting using Qspec,²² a cut-off value of 0.05 for false discovery rate was used for statistical significance. For all protein identifications, FDR was applied using a cut-off value of 0.01 to minimize false positives. See the Materials and Methods and Results sections for additional details of quantitation and statistical evaluation.

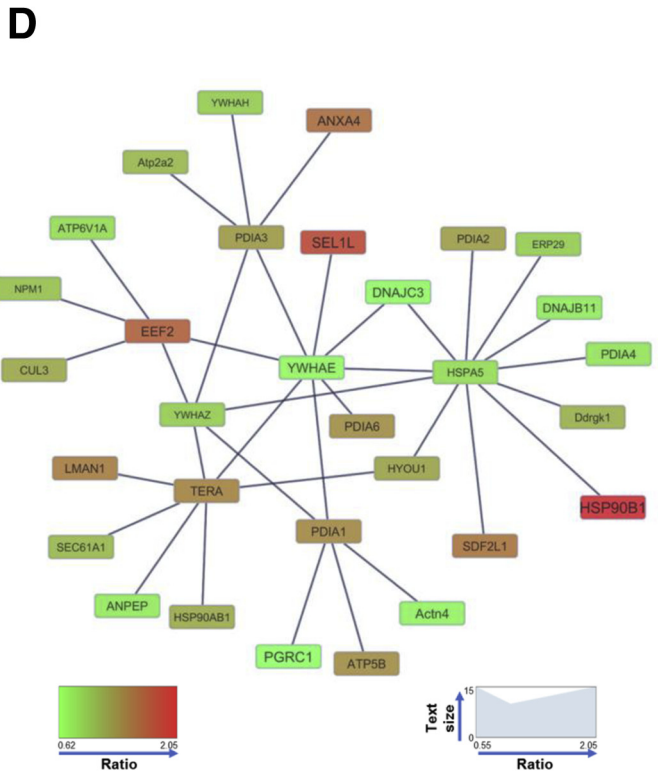
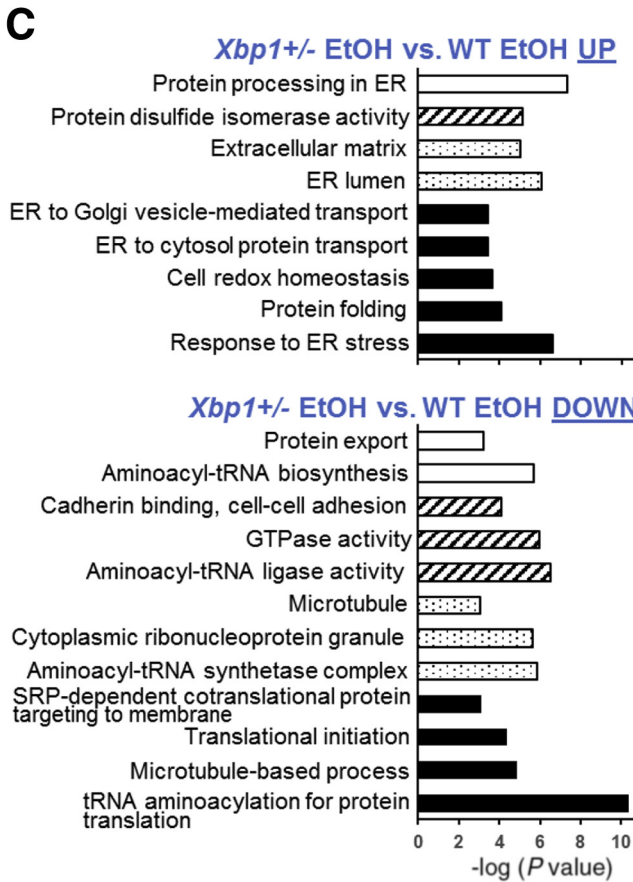
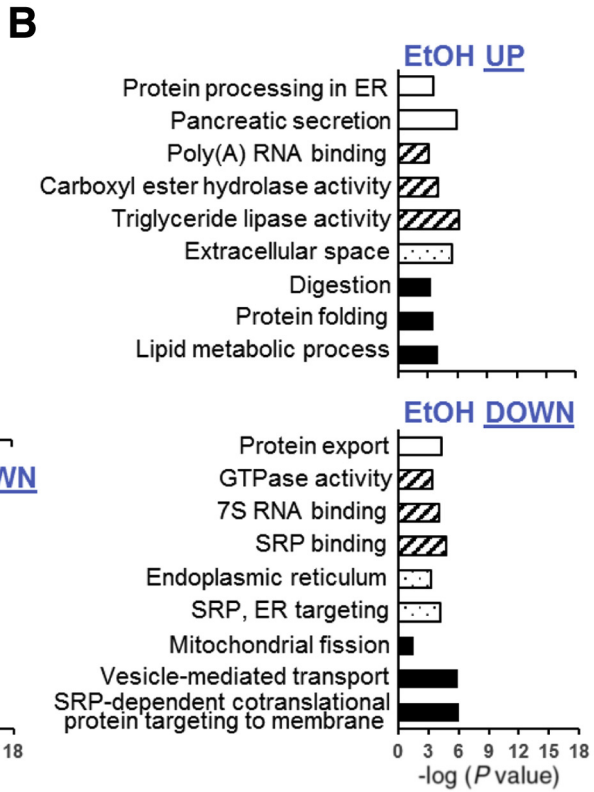
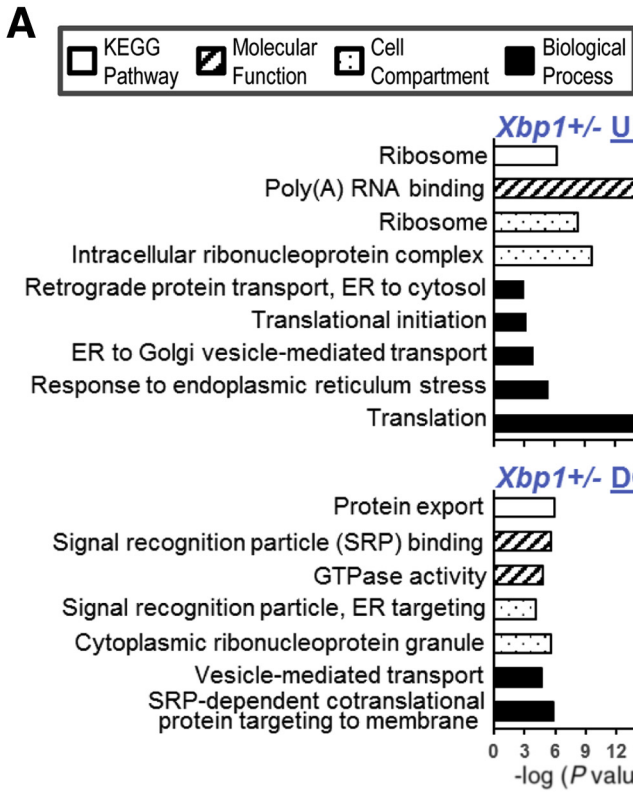
All authors had access to the study data and reviewed and approved the final manuscript.

Results

Ethanol Feeding and XBP1 Insufficiency Promote Redox Changes in ER Proteins

For these studies, we used *Xbp1*^{+/-} and littermate WT mice (Balb/c background), intragastrically fed control or

ethanol-containing diets. We reported that ethanol feeding in rats and mice induced pancreatic ER oxidation, mild ER stress, and marked up-regulation of sXBP1, but not acinar cell pathology.¹² In contrast, in pancreas of *Xbp1*^{+/-} mice, ethanol-induced up-regulation of sXBP1 was blocked, leading to exacerbated ER stress, sustained activation of the Protein kinase RNA-like Endoplasmic Reticulum Kinase - CCAAT/-enhancer-binding protein Homologous Protein (PERK/CHOP) branch of the UPR, limited expression of ER chaperones and foldases, and increased ER oxidation, associated with acinar cell pathology. Compared with WT mice, ethanol-fed *Xbp1*^{+/-} mice showed fewer zymogen granules (containing digestive enzymes), impaired secretory capacity, accumulation of autophagic vacuoles, and cell necrosis.^{12,14} We subsequently found that a subthreshold proinflammatory signal (3 hourly intraperitoneal injections of 1 μ g/kg cerulein), which was very mild when administered to ethanol-fed WT mice, triggered an acute pancreatitis response in *Xbp1*^{+/-} mice. For example, cerulein increased blood lipase levels (a marker of pancreatitis) by only 2.3-fold in ethanol-fed WT mice, but by 6.6-fold in ethanol-fed *Xbp1*^{+/-} mice. These data suggest that the



impact of ethanol diet-induced redox or other changes on ER protein structure in WT mice is limited by an sXBP1-mediated adaptive response that prevents acinar cell pathology in WT animals.¹²

Here, we sought to elucidate whether ethanol intake perturbs ER protein structure more in *Xbp1*^{+/-} mice than in WT mice. Mice were fed control and ethanol-containing diets for 6 weeks, as in our previous study,¹² then pancreata were harvested, and ER fractions were processed (Figure 1). We first examined the redox status of ER proteins by OXICAT. This method reliably quantifies the %-ox as the ratio of disulfide-bonded (or otherwise reversibly oxidized) to free sulfhydryl cysteines.¹⁵ In Supplementary Table 1, we report a novel exocrine pancreatic redox proteome, comprising 500 peptides from 264 proteins, mainly from ER and vesicles (both luminal and membrane-associated). Proteins present were involved in biological processes such as translation (66 of 264; 25.0%), transport (56 of 264; 21.2%), oxidation reduction (23 of 264; 8.7%), proteolysis (15 of 264; 5.7%), and protein folding (10 of 264; 3.8%), as indicated by DAVID analysis.^{23,24} We found that peptides from highly disulfide-bonded ER proteins, such as ribonuclease 1, were almost exclusively labeled with heavy ICAT, indicative of high (>90) %-ox, whereas those from peripherally ER-associated proteins were as low as ~30% (not shown).

To evaluate the influences of experimental conditions, we calculated the peptide %-ox values in *Xbp1*^{+/-} relative to WT mice (Figure 2A and Supplementary Table 1), and ethanol relative to control feeding (Figure 2B and Supplementary Table 1) in peptides that were detected and quantified 3 times or more during analysis of replicates, with all data comparisons, with *P* < .1 included for comparison. A log₁₀ plot of the *Xbp1*^{+/-}/WT data distribution showed changes in many ER proteins, including statistically significant lowered %-ox in the abundant digestive enzyme trypsinogen 7, which is attributed to impaired disulfide bonding (Figure 2A and Supplementary Table 1). In contrast, ethanol relative to control feeding increased %-ox in virtually all proteins, with the largest shifts at sites in *Snd1*, *Rab3d*, and *Ostc* (Figure 2B), all of which were statistically significant (Supplementary Table 1). To illustrate major shifts in redox status, we plotted the proportional distribution of peptide %-ox in each condition

(Figure 2C). WT control peptides were distributed with a large symmetric peak at ~70%-ox and a smaller peak near 100%-ox. In ethanol-fed WT mice, the main peak was higher at ~80%-ox. Together, data in Figure 2B and C establish a central finding of this study: that the ethanol diet shifts many ER proteins toward a more oxidizing redox status. In contrast, in control-fed *Xbp1*^{+/-} mice, the main peak was shifted to less oxidized levels (~50%). This reducing shift reflects the preponderance of data below the zero line in the y-axis of Figure 2A. Consistent with this, in ethanol-fed *Xbp1*^{+/-} samples, the peak was shifted toward a highly oxidizing (~90%-ox) value, indicating more severe ethanol-induced oxidation in the *Xbp1*^{+/-} mice ER. These results are consistent with our previous observations that ethanol feeding reduces the ratio of reduced/oxidized glutathione and induces reversible oxidation of the ER foldase Pdi/P4hb in *Xbp1*^{+/-} mice.¹² Figure 2D illustrates the ethanol-induced %-ox increase in ER-associated peptides. Thus, ethanol feeding increased peptides with >80%-ox from ~25% to ~45% in WT mice. This contrasted with a much larger increase, from ~20% to ~80% in *Xbp1*^{+/-} mice (Figure 2D). Thus, many (non-disulfide-bonded) sulfhydryls in the ER of *Xbp1*^{+/-} mice are highly susceptible to ethanol-induced oxidation, some of which may represent aberrant disulfide bonds.

Many peptides from pancreatic ER proteins showed significant %-ox fold-changes in response to *Xbp1*^{+/-} vs WT genetic status, ethanol vs control feeding, or both (Supplementary Table 1). Notably, several of these proteins are from the serine hydrolase enzyme family, abundant in the ER proteome of the pancreatic acinar cell. Disturbances in ER folding of these highly abundant digestive enzymes likely leads to protein misfolding and ER stress. Moreover, redox changes in proteases or lipases could detrimentally affect their expression levels, localization, or intracellular activity in acinar cells. Cys-containing peptides from digestive enzymes such as *Prss1* show *Xbp1*^{+/-} genotype-dependent reducing shifts and ethanol feeding-dependent increases in %-ox (Supplementary Table 1 and Figure 2B), representing bidirectional modulation of disulfide bonds. Thus, the peptide IVGGYTCR near the amino termini of *Prss1* (highly expressed in Balb/c mice) showed a 1.57-fold increase in %-ox in ethanol-fed vs control-fed mice. Independently, the %-ox of the peptide VGCPTEDTGK, containing Cys266

Figure 4. (See previous page). Changes in pancreas ER protein levels shown by proteomic data. In-gel digests were performed to identify FP-desthiobiotin-labeled peptides (shown in Supplementary Table 4), and many unlabeled proteins, as described in the *Results* and *Materials and Methods* sections. Spectral counts of all unmodified proteins identified in flow-through of the OXICAT experiment (see Supplementary Tables 2 and 3 for modified peptides) also were incorporated into this analysis. (A) Spectral counts of combined *Xbp1*^{+/-} vs WT mice pancreas ER proteins were quantitated label-free by spectral counting (shown in Supplementary Table 5) and subjected to DAVID analysis to identify gene ontology changes. (B) Spectral counts of combined ethanol- vs control-fed mice pancreas ER proteins were quantitated by spectral counting (shown in Supplementary Table 6) and subjected to DAVID analysis. (C) Gene ontologic changes obtained by comparison of ethanol-fed *Xbp1*^{+/-} with ethanol-fed WT mice by spectral counting and DAVID analysis. (D) Cytoscape interaction network. An interaction network was established among 6 ER stress response proteins significantly increased in ethanol-fed *Xbp1*^{+/-} vs ethanol-fed WT mice (*P4hb*, *Pdia3*, *Pdia4*, *Pdia6*, *Sel1l*, and *Eef2*), within the context of the larger network of compared proteins obtained by LC-MS/MS. Legends show the fold-change of each protein as a color range from green (decreased) to red (increased), and by a range of text sizes from small (decreased) to large (increased). GTP, guanosine triphosphate; SRP, signal recognition particle; tRNA, transfer RNA.

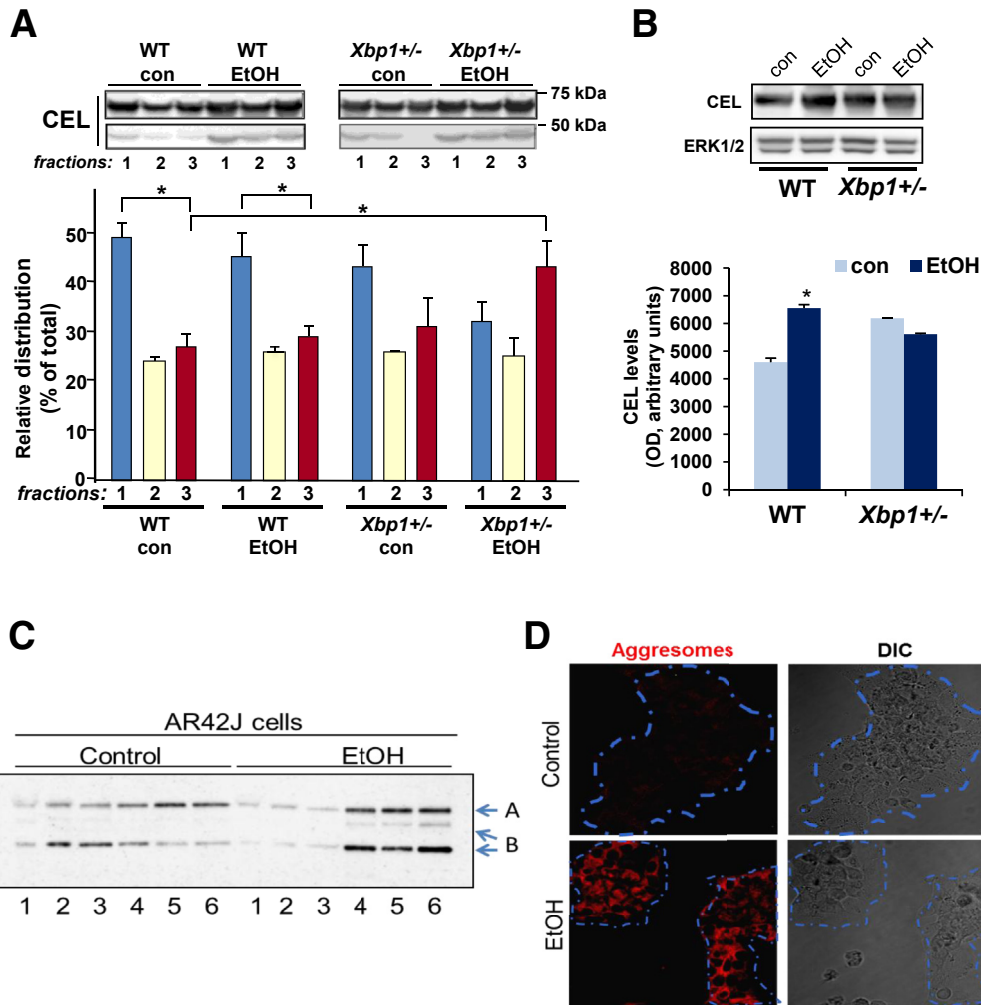


Figure 5. Cel protein is differentially distributed among subcellular fractions and total pancreas tissue from ethanol-fed *Xbp1*^{+/-} or WT mice, and in cultured AR42J pancreatic acinar cells exposed to ethanol. Pancreas tissue was harvested and fractionated as in Figure 1, from WT or *Xbp1*^{+/-} mice fed control (con) or ethanol (EtOH) diets for 5–6 weeks. Fractions were obtained by centrifugation at (1) 1500 × g; (2) 10,000 × g; and (3) 85,000 × g. (A) Cel (70 kilodalton) protein was analyzed by Western blot (upper panels), and quantitated in the different fractions (20 μg/lane) in the graph (lower panels) (optical density, means ± SEM, n = 3). A Cel protein fragment of ~48 kilodaltons also was detected in the fractions. (B) Cel protein expression is enhanced in total pancreas tissue upon EtOH feeding or in the *Xbp1*^{+/-} mice. Pancreas tissue was harvested from control- or EtOH-fed WT or *Xbp1*^{+/-} mice, and total proteins extracted with RIPA buffer without further fractionation. Cel protein and extracellular signal-regulated kinase 1/2 as a loading control were analyzed by Western blot in tissue extract (40 μg/lane). In the graph, the optical density of Cel bands was quantitated relative to total extracellular signal-regulated kinase protein; data indicate means ± SEM, n = 3. (C) AR42J cells were cultured for 48 hours in control medium (K12 medium supplemented with 12% fetal bovine serum) alone or with 100 mmol/L EtOH. ER membrane fractions were obtained by centrifugation of hypotonically lysed cells at (1) 150 × g; (2) 750 × g; (3) 1300 × g; (4) 5000 × g; (5) 12,000 × g; and (6) 100,000 × g. Cel protein in the fractions (10 mg/lane) was analyzed by Western blot. Arrows indicate the following: (A) Rat Cel, ~70 kilodaltons; and (B) Cel fragments, ~40–60 kilodaltons. (D) Ethanol-induced aggregate formation in AR42J cells. Cells were kept untreated or treated with 100 mmol/L EtOH for 48 hours, and then cellular aggregates were visualized in a confocal microscope using the PROTEOSTAT Aggresome detection kit (ENZ-51035; Enzo Life Sciences, Farmingdale, NY). Red fluorescence (left panels) indicates aggregates; corresponding differential interference contrast microscopy images are shown (right panels). *, P value less than .05 by student's t test.

from Cel (an abundant lipase produced by acinar cells), was modestly increased by ethanol feeding (Supplementary Table 1 and Figure 2B).

Notably, Cys modification of some peptides precluded them from OXICAT analysis because their sulfhydryls could no longer be labeled. We found that Cel Cys266 was reversibly oxidized (sulfenylated) by ethanol feeding by

analysis of flow-through from the OXICAT experiment, as described in the next section.

Peptides With Modified Cysteine Residues in the ICAT Affinity Column Flow-Through

Cys residues are important loci for protective, redox signaling, or damaging modifications.²⁵ Although the

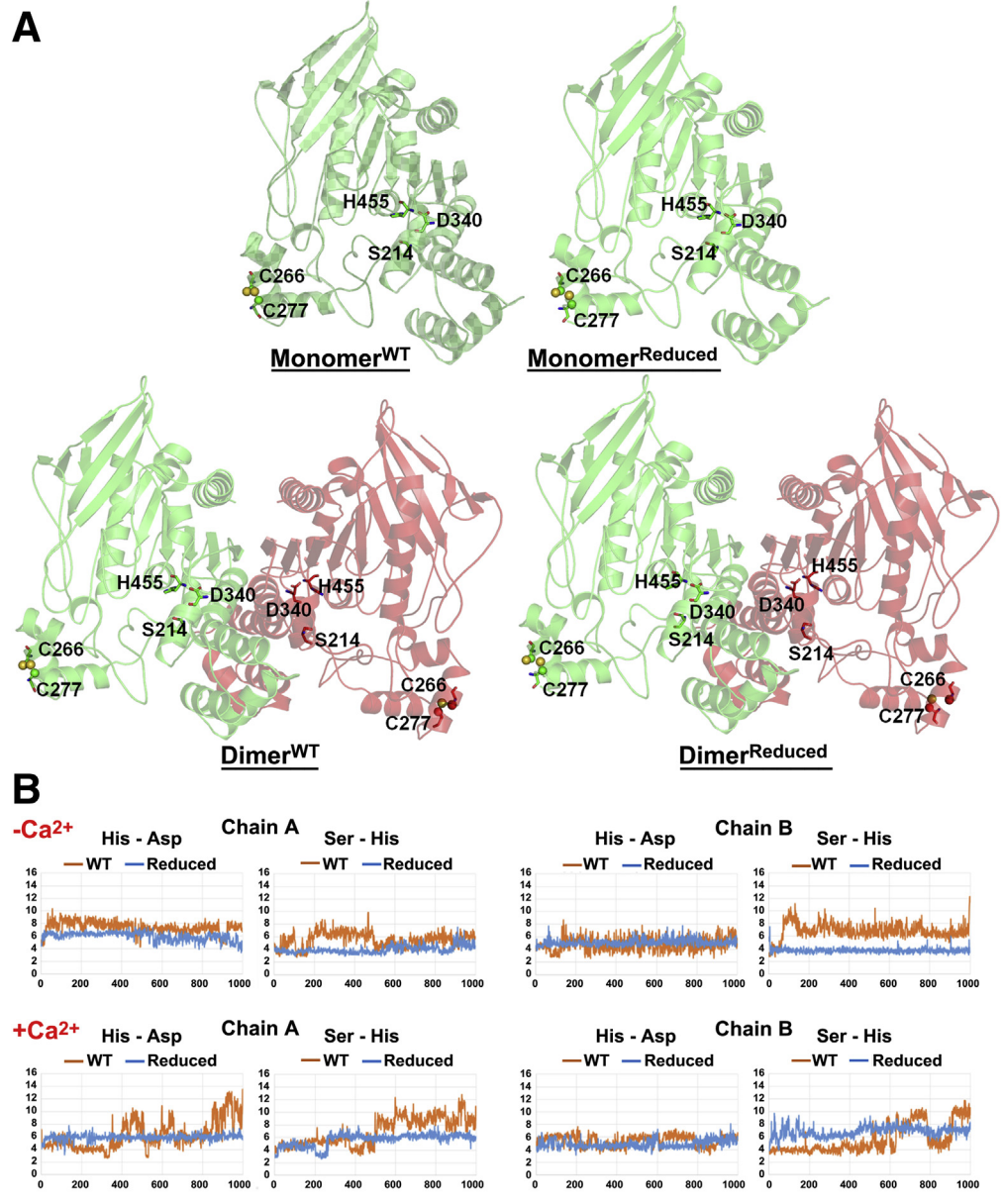


Figure 6. Cel structure responds to Cys266 disulfide disruption by stabilizing activity and dimers. (A) Monomeric and dimeric 3-dimensional structures of the WT and reduced forms of Cel. The *upper pair* of structures illustrate that disruption of the disulfide bond, Cys266–Cys277, in Cel is consistent with preservation of catalytic activity because it has little to no effect on the residue spacing within the catalytic triad. The *lower pair* of structures depict the enhanced interaction at the protomer–protomer interface that result from disrupting the Cys266–Cys277 disulfide bond in Cel, consistent with enhanced formation of a Cel–Cel dimer. (B) His–Asp and Ser–His distance plots in WT and reduced dimer (a) without Ca²⁺; and (b) with Ca²⁺.

OXICAT method allowed us to determine the proteins with reducible Cys, a subset of proteins may have post-translational modifications rendering these residues unlabeled. To identify modified Cys residues, we screened, without further enrichment, flow-through of the avidin columns after ICAT-biotin labeling by LC-MS/MS for peptides with reversible glutathionyl-, farnesyl-, and acetyl-labeled Cys, and acetyl-Lys containing peptides (Supplementary Table 2). Although Hbb-b1 acetyl-Lys60, was ubiquitous, most were complementary (unique) between conditions. However, some occurred selectively, suggesting preferential formation under certain conditions in vivo. For example, Nav1 acetyl-Lys1832 was absent from ethanol-fed *Xbp1*^{+/-} mice but present in the other 3 groups under study (Supplementary Table 2).

We also looked for sulfenyl, sulfinyl, sulfonyl, and nitrosyl Cys modifications that interrupt disulfide bonds (Supplementary Table 3). Some Cys-oxidized peptides, such as ITEFCHR from the b' (chaperone) region of Pdi/P4hb and LSTLPSDFCGLTHLVK from Lrrc59 (Supplementary Table 2) appeared in both control- and ethanol-fed samples, suggesting constitutive roles in these proteins. However, Rab1A was sulfenylated at Cys123, a residue homologous to Cys126 previously reported in the human cervical cancer cell line, HeLa cells,²⁶ in ethanol-fed WT mice only. A peptide from Bptf had Cys oxidation/nitrosylation in ethanol-fed WT and (both control- and ethanol-fed) *Xbp1*^{+/-} mice. Finally, peptides from Eef1a1, Acvr1b, and Cel were selectively oxidized/nitrosylated in ethanol-fed mice, suggesting their selective modification or damage under this condition. An Mbd-1

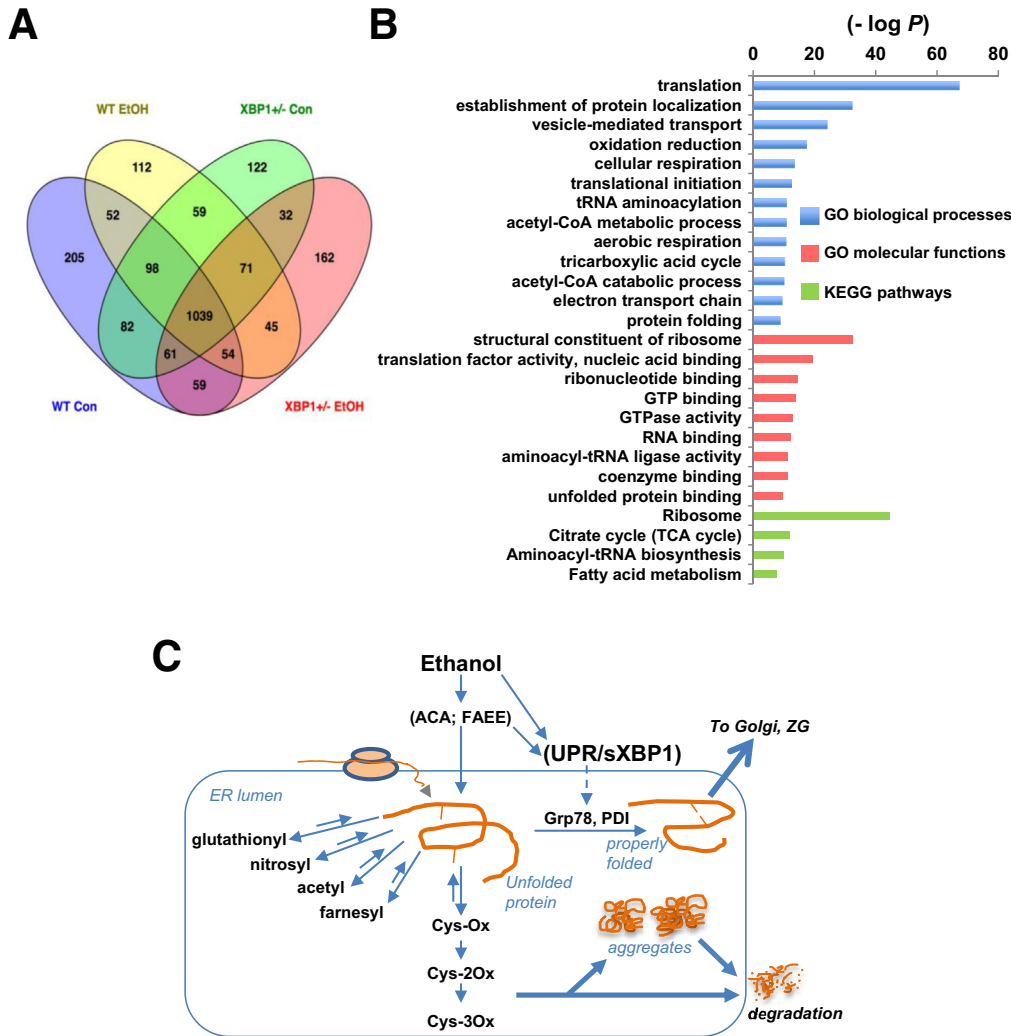


Figure 7. The pancreatic ER proteome. WT and *Xbp1*^{+/-} mice were fed control (con) or ethanol (EtOH) diet for 5–6 weeks. At the end of the feeding period, pancreata were harvested and proteomic analysis was performed on ER fractions. (A) Venn diagram showing the overlap in proteins associated with each experimental group. (B) Gene ontology (GO) analysis of the shared genes between all 4 groups. The major Gene ontology terms of Biological Processes and Gene Functions and KEGG pathways are shown according to log₁₀ of the *P* value. (C) Model depicting protein folding and packaging, mediated by chaperones and oxidoreductases. Ethanol promotes a pathway for which protective modifications and oxidative/nitrosative (putative signaling modifications) exist and damage ultimately occurs, leading to protein aggregation and degradation. KEGG, Kyoto Encyclopedia of Genes and Genomes.

peptide, found only in ethanol-fed *Xbp1*^{+/-} mice, had 3 Cys residues modified by both glutathionyl/acetyl and sulfonyl/nitrosyl groups. Two peptides, 1 from the C-terminal region of Ift122 and the other in the BIR2 domain of Xiap that interacts with caspases, contained multiple glutathionyl-, farnesyl-, or acetyl-Cys residues in control-fed WT mice (Supplementary Table 3), but were oxidized or nitrosylated at the same sites only in ethanol-fed *Xbp1*^{+/-} mice (Supplementary Table 2). These data provide evidence that ethanol feeding and XBP1 deficiency favor multiple changes in Cys residues in ER proteins, possibly related to the severe ER stress and pathologic effects in acinar cells induced by the combination of ethanol feeding and XBP1 insufficiency.^{5,12}

Cel Is a Unique Serine Hydrolase Active in Pancreas ER, and Severe ER Stress Favors its Dimerization

Most digestive enzymes are synthesized as zymogens lacking activity. As a first step toward identifying a functional correlate of redox alterations, we examined whether ER stress associated with XBP1 deficiency or ethanol

feeding altered serine hydrolase activity. These assays could show whether changes in ER %-ox lead to inappropriate intracellular activation of proteases (eg, trypsin), a hallmark of pancreatitis.^{27,28} We used fluorophosphonate (FP) desthiobiotin, a probe that reacts selectively with catalytic Ser in active serine hydrolases. Reactive ER proteins, mainly *Cel*, were detected and displayed by Western blot (Figure 3).

As shown in Figure 3A, FP desthiobiotin reacted strongly with an ~140-kilodalton upper and an ~70-kilodalton lower band. Both intense bands corresponded to a single major serine hydrolase activity (ie, the ~70-kilodalton *Cel*; as determined by in-gel digest and LC-MS/MS; see later), indicating active monomers and dimers (Figure 3A). We quantitated all of the upper and lower gel bands by densitometry (Figure 3B). The ratio of dimeric- to monomeric-labeled *Cel* was ~0.25 in control- and ethanol-fed WT and control-fed *Xbp1*^{+/-} mice, but substantially higher, ~0.42, in ethanol-fed *Xbp1*^{+/-} mice (Figure 3C). Several low-intensity bands of ~15–65 kilodaltons (Figure 3D), which could be *Cel* fragments or distinct, low-activity serine hydrolases, were increased (~1.4- to 1.7-fold) by ethanol feeding in both WT and *Xbp1*^{+/-} mice (Figure 3E).

To identify FP-desthiobiotin-labeled and -unlabeled proteins, proteins were separated by electrophoresis, Coomassie-stained, in-gel digested with trypsin, and analyzed by LC-MS/MS. Of note, the patterns of Coomassie-stained bands and the distributions of spectral counts across gel slices were similar, indicating that a similar depth of mass spectral analysis was achieved under each condition. The peptides covalently linked to FP desthiobiotin identified by this approach, including a 34-aa Cel peptide labeled at its catalytic Ser18, are presented in [Supplementary Table 4](#). Although the Cel peptide was detected in both the 70- and 140-kilodalton gel slices in the ethanol-fed *Xbp1*^{+/-} mice (corresponding to the strong bands in [Figure 3A](#)), it was observed at a low gel position (16–24 kilodaltons) in WT, suggesting that active Cel was selectively degraded in these mice. Although Cel was the only active serine hydrolase we found, other proteins with peptides labeled at Ser or Tyr residues were detected and are listed in [Supplementary Table 4](#).

Ethanol Feeding and XBP1 Insufficiency Alter the Protein Expression Levels in ER Fractions

We next assessed the relative expression levels of 1568 ER proteins identified in LC-MS/MS analysis of the (flow-through of the) OXICAT and serine hydrolase experiments. In the first analysis, we pooled data sets to analyze *Xbp1*^{+/-} vs WT, and EtOH vs control-fed mice. Data summarized in [Supplementary Table 5](#) show that the *Xbp1*^{+/-} genotype induced significant changes in 100 proteins, with 63 going up and 37 going down. Nineteen and 25 proteins went up or down, respectively, by at least 1.5-fold. Notably, dynactin and dynein, components of microtubule-dependent vesicular trafficking, were increased, yet multiple tubulins were decreased, suggesting uncoupling of this pathway of zymogen granule apical targeting.²⁹ Shown in [Figure 4A](#) are gene-ontologic categories (Kyoto Encyclopedia of Genes and Genomes pathways, molecular functions, cellular compartments, and biological processes) of proteins increased or decreased in ER in response to *Xbp1*^{+/-} genotype, as determined by DAVID analysis. Notable changes included increased ribosomes and other RNA-binding proteins, and proteins involved in endoplasmic reticulum-associated degradation (ERAD), translation, ER-to-Golgi vesicle-mediated transport, and the response to ER stress. Proteins that decreased included signal recognition particle components, guanosine triphosphatase, tubulins, and ribonucleoprotein granule proteins.

As shown in [Supplementary Table 6](#), ethanol feeding also changed the levels of proteins in the ER fraction, inducing 20 proteins to increase (4 at least 1.5-fold) and 31 to decrease (30 to 0.67-fold or less). Many of the increased proteins were secreted enzymes or ER luminal proteins, whereas the reduced proteins included several vesicular trafficking and ER regulatory proteins. The important altered ontology categories are shown in [Figure 4B](#).

[Supplementary Tables 5](#) and [6](#) also list several ER-associated proteins that were redistributed into gel slices different from their predicted MWs. Those proteins

were statistically increased or diminished in higher-MW complexes or degraded forms. The effects of ethanol feeding and the *Xbp1*^{+/-} genotype were similar and included increases in 125- to 150-kilodaltons complexes, and losses of signal recognition particle components Srp68 and Srp72, and the RNA helicases Ddx3x and Ddx3y.

To determine the selective unmasking effect of the impaired UPR condition on the ethanol feeding-induced changes, our data allowed us to compare the relative levels of 777 proteins in ethanol-fed *Xbp1*^{+/-} and ethanol-fed WT animals. By this analysis, a total of 38 proteins were higher, and 73 were lower in the ethanol-fed *Xbp1*^{+/-} ER samples. These proteins are listed in [Supplementary Table 7](#), and the Gene ontology categories affected are listed in [Figure 4C](#). Increased categories included ER stress response, cell redox homeostasis, ERAD, and protein folding. Reduced levels of signal recognition particle, microtubule, and aminoacyl transfer RNA synthases persisted in the ethanol-fed *Xbp1*^{+/-}, compared with ethanol-fed WT samples. To further illustrate connections between 6 increased proteins involved in the response to ER stress (Pdia1, Pdia2, Pdia3, Pdia6 Eef2, and Sel1l) and the larger network of changes unmasked under this condition, we developed an interconnected network of interactions using Cytoscape (www.cytoscape.org/),³⁰ shown in [Figure 4D](#).

Selective Cel Dimer Retention in ER of Ethanol-Fed Xbp1^{+/-} Mice

In view of the evidence of ER Cel dimer formation ([Figure 3A](#) and [C](#), [Supplementary Table 6](#)), together with previous reports,³¹ and our data of ER retention of secreted proteins including Cel ([Figure 4](#)), we next measured the amounts of Cel in membranes enriched for zymogen granules (fraction 1), mitochondria (fraction 2), and ER microsomes (fraction 3) by Western blot ([Figure 5A](#)). Full-length Cel (~70 kilodaltons) was found in the 3 fractions ([Figure 5A](#), quantitated in the lower panel). In addition, a smaller Cel polypeptide of ~40 kilodaltons was enhanced in all fractions in ethanol-fed mice ([Figure 5A](#)). As expected, significantly more full-length Cel proteins appeared in zymogen granule than in ER fractions in control-fed WT mice, and ethanol feeding had only a minor effect on Cel distribution between fractions in these mice. A pronounced shift to the ER emerged only in ethanol-fed *Xbp1*^{+/-} mice, suggesting that ethanol feeding-induced changes exacerbated by inadequate UPR were responsible for Cel retention in ER. Consistent with its trafficking, packaging, and/or release being impeded, the abundance of Cel protein increased modestly (~1.3-fold) in ethanol-fed WT and all *Xbp1*^{+/-} tissue homogenates ([Figure 5B](#)).

As a second model of ethanol-induced pancreas ER dysfunction, we examined whether Cel was retained in an ER fraction from cultured acinar AR42J cells. Cells were cultured for 48 hours in control media either alone or supplemented with 100 mmol/L ethanol. Then, cells were hypotonically lysed and fractionated. Consistent with data in [Figure 5A](#) and [B](#), Western blot analysis of membrane fractions showed that Cel is retained within an ER microsomal

fraction even with acute ethanol treatment. Again, ethanol promoted Cel cleavage into an ~40 kilodalton polypeptide, especially in the ER fraction (Figure 5C). Cel tends to form aggregates when its secretion is impaired, such as when its C-terminal extension is mutated.^{6,32}

To determine whether ethanol induced complex formation in AR42J cells, cultures were exposed to 100 mmol/L ethanol for 48 hours, then fixed and stained with a protein aggresome detection kit. Results show selective ethanol-induced complex formation throughout the cytoplasm of AR42J cells (Figure 5D).

Modeling of the Cel Monomers and Dimers to Assess the Structural Effect of Redox Modifications on Cel

Cel activity produces toxic fatty acid ethyl esters (FAEE) in acinar cells exposed to ethanol, and recently was highlighted as a therapeutic target to modulate ethanol pancreatitis.³³ Indeed, a specific small-molecule inhibitor that binds to the Cel active site attenuated the severity of experimental pancreatitis induced by promoting ethanol metabolism to FAEE.³³ This report examines the molecular structure of the Cel active site in detail, underscoring its importance. Here, a Cel peptide containing Cys266 that typically resides in a disulfide bond was selectively oxidized in our ethanol-fed samples. To assess the requirement of the Cys266–Cys277 disulfide bond for Cel activity, we studied inter-residue distances of the Ser214–Asp340–His455 (catalytic triad) in monomeric forms of both WT (Monomer^{WT}) and (C266A/C277A) double-mutant (Monomer^{Reduced}) mouse Cel (Uniprot Q64285). Because Cel formed dimers under ethanol-fed conditions associated with a redox imbalance, we also studied the atomic structures of dimeric WT and C266A/C277A Cel (Dimer^{WT} and Dimer^{Reduced}, respectively). Monomeric and dimeric structures obtained (shown in Figure 6A) were relaxed in molecular dynamics simulations, both with and without 300 μmol/L Ca²⁺ to approximate the physiologic ER Ca²⁺ concentration. In structural stability analysis, average His–Asp and Ser–His distances calculated without Ca²⁺ increased from 6.27 and 3.71 Å in Monomer^{WT}, to 6.82 and 10.51 Å in Monomer^{Reduced}, respectively (data not shown). This loss of stable Ser–His distance in the –Ca²⁺ condition was selective for the Monomer^{Reduced} because His–Asp and Ser–His distances remained close to ~4 Å (consistent with activity) under both –Ca²⁺ and +Ca²⁺ conditions in the Monomer^{WT}. These data suggest that the activity of Monomer^{WT} is more stable than Monomer^{Reduced} in a low-Ca²⁺ environment such as the cytoplasm.

In contrast, measurement of His–Asp and Ser–His distances in individual protomer chains A and B of dimers showed that a stable catalytic triad tended to be more advantageous in Dimer^{Reduced} than in Dimer^{WT}, both in the presence and absence of Ca²⁺ (Figure 6B), suggesting relatively more stable activity of Dimer^{Reduced} than Dimer^{WT} in either the cytoplasmic or ER environment. Moreover, in analysis of protomer:protomer binding energy there is tighter association in Dimer^{Reduced} than in Dimer^{WT},

owing to more polar contacts (53 vs 36 hydrogen bond, and 10 vs 2 salt bridge interactions, respectively) across the protein–protein interface. In summary, our structural modeling data and simulations indicate that the C266A/C277A double-mutant Cel achieves lower energy (stabilizes) and retains catalytic activity as a dimer. These data imply that ethanol-fed conditions favor disrupted Cys266–Cys277 disulfide bonds, leading to stabilized Cel–Cel dimers that retain activity.

Murine Pancreas ER Proteome and a Model of Ethanol-Induced Redox-Mediated Pancreas Pathology

LC-MS/MS analysis of pancreatic tissues from control- and ethanol-fed WT and *Xbp1*^{+/-} mice provided many unlabeled peptides that were compiled into a novel murine pancreas ER proteome (Figure 7A and B and Supplementary Table 8). Many serine hydrolases including pancreatic triglyceride lipases (Pnlip, Pnlipr2) and zymogens of elastase (Cela1a, Cela21, Cela2b), chymotrypsin (Ctrb1), and trypsin (Prss2; 2210010C04Rik) were identified.

Figure 7C illustrates a working model fitting our data, in which ethanol promotes oxidative damage of secreted proteins as they pass through ER. Some of the Cys sulfhydryls that represent damage sites may be protected by alternative modifications. Some redox changes, such as in Cel, promote higher-order structures such as dimers, and complex and/or aggregate formation and degradation, which we propose to represent key early changes leading to pancreatic pathology. A fully functional UPR/sXBP1 response aids the ER to cope with ethanol-induced redox changes and other post-translational modifications. However, a dysfunctional UPR associated with XBP1 deficiency, promotes ethanol-induced pathology.

Discussion

The major shifts in %-ox induced by ethanol feeding in peptides from mouse pancreatic ER illustrate pro-oxidizing effects of ethanol that were exacerbated in mice with a defective UPR (XBP1-deficient, *Xbp1*^{+/-} mice). ER from control-fed *Xbp1*^{+/-} mice showed a reducing shift, consistent with impaired disulfide bonding/protein folding. These results underscore established links between the IRE1–XBP1 branch of UPR and expression of disulfide bonding enzymes such as protein disulfide isomerase and chaperones such as Grp78.³⁴

We found individual peptide %-ox changes in many proteins, including foldases (eg, Pdia1), digestive enzymes (eg, trypsinogen), and vesicle trafficking proteins (eg, Rab3d). A large oxidizing shift was found in Rab3d Cys184, a residue conserved within the Rab3 subfamily and shared with Rab33A.³⁵ Oxidation at this site may compromise interaction with effector(s), altering Rab3d functions in the regulation of digestive enzyme secretion,³⁶ zymogen granule formation,³⁷ or Golgi structure and ER-to-Golgi traffic³⁸ in acinar cells. Likewise, a large oxidizing shift in the transcriptional co-activator Snd1 may modulate its signaling or its emerging role in stress granule function³⁹ in

ethanol-fed and/or *Xbp1*^{+/-} mice. Further study of specific changes in %-ox that were shown here may elucidate defects of trafficking and organellar function in the pathologic sequence of pancreas disease.³

Protein glutathionylation of Cys residues prevents irreversible modifications,^{40,41} as previously modeled in specific proteins such as Na-K-adenosine triphosphatase (ATPase)⁴² and locations including ER.⁴³ Ethanol-induced protein glutathionylation was shown in liver,^{44,45} but not in pancreas. We searched for Cys glutathionylation, farnesylation, acetylation, oxidation/nitrosylation, and Lys acetylation in flow-through samples from OXICAT peptide isolation. Some modifications, such as a trioxidized peptide within Lrrc59, were found constitutively (ie, in all the flow-through samples). No peptides were both protectively modified in the ethanol fed or *Xbp1*^{+/-}, and nitrosylated/oxidized in the control or WT mice. These results suggest that UPR supports protective modifications to prevent ethanol-induced S-nitrosylation/oxidation, and justify future, more comprehensive, analysis of these modifications.

We also monitored serine hydrolase activity in pancreas ER that might emerge as a final proximal event or point of no return in triggering pancreatitis. Our data identify Cel as the only prominent serine hydrolase activity in ER, and its selective dimerization in ethanol-fed *Xbp1*^{+/-} mice. Cel, among a few other enzymes, is modestly (1.2- to 1.5-fold) retained in ER of acinar cells during ethanol feeding. Undefined trafficking defects and secretory blockade in the acinar cell are hypothesized to culminate in pathologic proenzyme activation during acute pancreatitis. Although intrapancreatic trypsinogen activation was long considered as a hallmark of pancreatitis, in recent years its importance as a definitive marker or causative factor has been questioned.²⁸ Because we did not observe active trypsin using the serine hydrolase activity probe, trypsinogen activation does not seem to play a role in our model of XBP1 deficiency- and ethanol feeding-induced acinar cell pathology. Instead, pancreatitis sensitizing mechanisms were associated with marked changes in ER protein oxidation and expression, and severe ER stress.¹² Our proteomic and molecular dynamics simulation data support the possible participation of Cel in the pathobiology of alcoholic pancreatitis.

Structural/functional alterations in Cel can mediate pathobiology of ethanol pancreatitis. Cel is synthesized in active form and hydrolyzes substances including triglycerides and cholesteryl esters. Furthermore, Cel FAEE synthase activity mediates pathologic changes in acinar cells by direct toxic actions of FAEE to mitochondria³³; free fatty acids liberated from triglycerides⁴⁶ and cholesterol from cholesteryl esters also may damage the pancreas. Consistent with prior electrophoretic, chromatographic,⁴⁷ and crystallographic⁴⁸ studies, our data show that active Cel is retained in ER and forms dimers. Although the role(s) of dimeric Cel remain(s) unknown, Cel dimer formation might nucleate more general protein aggregation. Toxic aggregate formation has been identified as a pathogenic role of mutant forms of Cel.^{6,49} We detected pronounced ethanol-induced aggregate formation in cultured AR42J

acinar cells. Selective degradation of Cel in the ER of WT but not *Xbp1*^{+/-} mice may reflect sXBP1-mediated expression of ERAD proteins.⁵⁰

Serine hydrolase probe labeled some other targets that need further study to ascertain their roles in pancreatic disease. For example, Creld2, an ER stress-responsive protein with a protein disulfide isomerase-like activity⁵¹ was labeled in all samples except the WT control, suggesting its fluorophosphonate sensitivity. Ethanol feeding and the *Xbp1*^{+/-} genotype drove changes in the levels of unlabeled ER-associated proteins, and redistributed some proteins into gel slices different from their predicted MW. Some of the proteins that increased in complexes also increased in lower MW, degraded forms, including signal recognition particle components Srp68 and Srp72, and the RNA helicases, Ddx3x and Ddx3y. Formation and degradation of Ddx3 complexes implied messenger RNA-protein structures associated with RNA splicing.⁵² We conclude that ethanol feeding, especially in *Xbp1*^{+/-} mice, favored protein complex formation and (perhaps inefficient) degradation (Figure 7C). Selective aggregation/and or degradation of proteins such as lipases, Snd1, or vigilin may disrupt homeostasis.

Further research is needed to understand the broad pattern of early protein changes in ER in response to ethanol feeding. The analysis of Figure 4B recapitulated findings of modest ER retention of secreted proteins such as trypsin, chymotrypsin, lipase, pancreatic lipase, elastase, and CEL. Salient proteins down-regulated by ethanol feeding including multiple signal recognition particle subunits and other proteins involved in vesicular trafficking, RNA binding, and membrane fission. Many categories of proteins up-regulated or down-regulated by ethanol feeding also were changed in the same direction in *Xbp1*^{+/-} vs WT mice. Taken together, data in Supplementary Tables 5-7 and Figure 4A and B indicate that both XBP1 deficiency and ethanol feeding induce selective alterations in ER proteostasis.

Here, we also specifically explored the effect of EtOH feeding in the context of *Xbp1*^{+/-} genotype, and observed changes that were unmasked in EtOH-fed *Xbp1*^{+/-} vs EtOH-fed WT mice. Proteins controlling ER stress response, and protein transport (eg, ERAD) were key proteins increased, whereas proteins involved in translation initiation, transfer RNA aminoacyltransferases, signal recognition particle components, T-complex chaperonins, multiple RNA helicases, and tubulins were decreased. Selective emergence of these changes in our model of impaired UPR suggests they are among the specific changes revised when the UPR is intact.

In our model designed to impair UPR resolution of ER stress, we mapped a network of ER stress proteins selectively unmasked by ethanol feeding in *Xbp1*^{+/-} mice to identify central nodes and unsuspected connections among the identified proteins using CytoScape. Within the resulting network, Hspa5/Grp78 (aka BiP) occupies a supermolecular cluster as previously described.⁵³ Chaperones such as Hsp90b1, Dnajb11, and redox folding proteins including Pdia2 and Pdia4 interact directly within this network that

also extends indirectly to Pdia1, Pdia6, and Hyou1/Grp170. Hyou1, a chaperone of the heat shock protein 70 family, acts as a nucleotide exchange factor for Hspa5, mediating its dissociation from client proteins.⁵⁴ Our data reinforce the function of Hyou1 at the intersection of protein vesicular trafficking and reverse translocation into the cytosol for degradation.⁵⁴

ERAD pathway components such as Tera/Vcp, Sel1 and Sdf1l, and Eef2, a major enzyme in translational elongation, are increased in the subnetwork, whereas various proteins such as Rab5C and phospho-regulatory 14-3-3 proteins are reduced. The central position of characteristically cytosolic 14-3-3 isoforms was unexpected, although these proteins promote forward secretion.^{55,56} Pdia1, Pdia3, and Pdia6 were previously detected in proteomic studies enriching 14-3-3 proteins to identify novel binding partners.^{57,58} Peripheral proteins in the network, such as Atp2a2 and ATP5c, play important roles in homeostasis, regulating Ca²⁺ sequestration and ATP production, respectively. Although the precise relationships between these proteins are not yet clear, our data infer a central functional importance of a novel phosphoregulatory network in the acinar cell response to ER stress promoted by ethanol feeding.

Some reversible modifications promoted by ethanol feeding, such as glutathionylation, are temporary and likely preserve Cys, whereas others such as progressive oxidation are permanent and represent accumulating damage. Among peptides selectively modified by glutathionylation/acetylation/farnesylation or oxidation/nitrosylation, we detected a Cel fragment oxidized at Cys266. Molecular dynamics simulations indicated that Cel retains activity, and dimer formation was promoted in the absence of the Cys266–Cys277 disulfide bond. Based on these findings, we propose that ethanol feeding-induced Cel Cys266 oxidation promotes Cel ER retention/dimerization, a cascade of events normally limited by sufficient XBP1 that underlies the emergence of pancreatitis in *Xbp1*^{+/-} mice. Modification of redox-sensitive Cys residues within other key molecules such as trypsin also may have pathologic consequences.

Although our results support the use of *Xbp1*^{+/-} mice as a model to determine ethanol-induced redox alterations, this study had some limitations. First, our LC-MS/MS study of OXICAT-labeled peptides had limited depth, suggesting that our data show a general mechanism, but not necessarily all the early targets of redox shift/modification. Next, because our Western blots using an antibody to Cel did not detect Cel–Cel dimers, we speculate that the antibody epitope impinges on the dimer interface, precluding its detection. Also, some changes we observed in response to ethanol feeding and/or *Xbp1*^{+/-} genotype may occur in the cytoplasm rather than in the ER.

Although ethanol and/or its metabolites induce toxicity in pancreatic acinar cells,^{33,59–62} relatively few heavy drinkers suffer pancreatitis. These disparate findings suggest that repair and/or defense pathways in pancreatic acinar cells are usually sufficiently robust to accommodate ethanol-induced insults. Recent epidemiologic studies implying that moderate alcohol consumption reduces the risk of pancreatitis^{63,64} may be explained by a low-dose ethanol-induced

induction of repair and/or defense pathways. However, an advantage of our model is that it allows us to examine changes that normally would have been repaired.

In conclusion, our data reinforce the concept that UPR is an important mechanism of pancreas and other organ defense and is partly responsible for redox control as recently hypothesized.⁶⁵ Proteins identified in the serine hydrolase discovery experiment and in flow through samples showed a range of changes and yielded a far more complete pancreatic ER proteome than previously published. Moreover, our study reinforces suspicions of Cel participation in ethanol feeding-induced pancreas damage and dysfunction, while not fully resolving whether altered Cel activity, which depends on the enzyme localizing with cofactors and substrates, or simply the presence of structurally altered protein, is required. Our results favor the conclusion that ethanol accelerates initiation of Cel degradation, but also inhibits its degradative flux. Further research is needed to learn the full scope of sensitizing changes and to clarify the contributions of Cel dimerization to later events. Study of the novel loci identified in this study where tissue damage is initiated will illuminate cascades of ethanol-induced dysfunction leading to the development of pancreatitis.

References

1. Lankisch PG, Apte M, Banks PA. Acute pancreatitis. *Lancet* 2015;386:85–96.
2. Setiawan VW, Pandol SJ, Porcel J, Wei PC, Wilkens LR, Le Marchand L, Pike MC, Monroe KR. Dietary factors reduce risk of acute pancreatitis in a large multiethnic cohort. *Clin Gastroenterol Hepatol* 2017;15:257–265 e3.
3. Gukovskaya AS, Pandol SJ, Gukovsky I. New insights into the pathways initiating and driving pancreatitis. *Curr Opin Gastroenterol* 2016. Epub ahead of print.
4. Pandol SJ. The exocrine pancreas. San Rafael, CA: Morgan & Claypool Life Sciences, 2011.
5. Lugea A, Waldron RT, Pandol SJ. Pancreatic adaptive responses in alcohol abuse: role of the unfolded protein response. *Pancreatol* 2015;15(Suppl):S1–S5.
6. Xiao X, Jones G, Sevilla WA, Stolz DB, Magee KE, Haughney M, Mukherjee A, Wang Y, Lowe ME. A carboxyl ester lipase (CEL) mutant causes chronic pancreatitis by forming intracellular aggregates that activate apoptosis. *J Biol Chem* 2016;291:23224–23236.
7. Kereszturi E, Szmola R, Kukor Z, Simon P, Weiss FU, Lerch MM, Sahin-Toth M. Hereditary pancreatitis caused by mutation-induced misfolding of human cationic trypsinogen: a novel disease mechanism. *Hum Mutat* 2009;30:575–582.
8. Kubisch CH, Sans MD, Arumugam T, Ernst SA, Williams JA, Logsdon CD. Early activation of endoplasmic reticulum stress is associated with arginine-induced acute pancreatitis. *Am J Physiol Gastrointest Liver Physiol* 2006;291:G238–G245.
9. Biczó G, Vegh ET, Shalbueva N, Mareninova OA, Elperin J, Lotshaw E, Gretler S, Lugea A, Malla SR, Dawson D, Ruchala P, Whitelegge J, French SW, Wen L, Husain SZ, Gorelick FS, Hegyi P, Rakonczay Z Jr, Gukovsky I, Gukovskaya AS. Mitochondrial dysfunction,

- through impaired autophagy, leads to endoplasmic reticulum stress, deregulated lipid metabolism, and pancreatitis in animal models. *Gastroenterology* 2018;154:689–703.
10. Lugea A, Gerloff A, Su HY, Xu Z, Go A, Hu C, French SW, Wilson JS, Apte MV, Waldron RT, Pandol SJ. Combination of alcohol and cigarette smoke induces endoplasmic reticulum stress and cell death in pancreatic acinar cells. *Gastroenterology* 2017;153:1674–1686.
 11. Cao SS, Kaufman RJ. Endoplasmic reticulum stress and oxidative stress in cell fate decision and human disease. *Antioxid Redox Signal* 2014;21:396–413.
 12. Lugea A, Tischler D, Nguyen J, Gong J, Gukovsky I, French SW, Gorelick FS, Pandol SJ. Adaptive unfolded protein response attenuates alcohol-induced pancreatic damage. *Gastroenterology* 2011;140:987–997.
 13. Pandol SJ, Gorelick FS, Gerloff A, Lugea A. Alcohol abuse, endoplasmic reticulum stress and pancreatitis. *Dig Dis* 2010;28:776–782.
 14. Lugea A, Waldron RT, French SW, Pandol SJ. Drinking and driving pancreatitis: links between endoplasmic reticulum stress and autophagy. *Autophagy* 2011;7:783–785.
 15. Leichert LI, Gehrke F, Gudiseva HV, Blackwell T, Ilbert M, Walker AK, Strahler JR, Andrews PC, Jakob U. Quantifying changes in the thiol redox proteome upon oxidative stress in vivo. *Proc Natl Acad Sci U S A* 2008;105:8197–8202.
 16. Sethuraman M, McComb ME, Heibeck T, Costello CE, Cohen RA. Isotope-coded affinity tag approach to identify and quantify oxidant-sensitive protein thiols. *Mol Cell Proteomics* 2004;3:273–278.
 17. Long JZ, Cravatt BF. The metabolic serine hydrolases and their functions in mammalian physiology and disease. *Chem Rev* 2011;111:6022–6063.
 18. Ozcan U, Cao Q, Yilmaz E, Lee AH, Iwakoshi NN, Ozdelen E, Tuncman G, Gorgun C, Glimcher LH, Hotamisligil GS. Endoplasmic reticulum stress links obesity, insulin action, and type 2 diabetes. *Science* 2004;306:457–461.
 19. Hess DA, Humphrey SE, Ishibashi J, Damsz B, Lee AH, Glimcher LH, Konieczny SF. Extensive pancreas regeneration following acinar-specific disruption of Xbp1 in mice. *Gastroenterology* 2011;141:1463–1472.
 20. Tsukamoto H, Mkrtychyan H, Dynnyk A. Intragastric ethanol infusion model in rodents. *Methods Mol Biol* 2008;447:33–48.
 21. Paulo JA, Kadiyala V, Lee LS, Banks PA, Conwell DL, Steen H. Proteomic analysis (GeLC-MS/MS) of ePFT-collected pancreatic fluid in chronic pancreatitis. *J Proteome Res* 2012;11:1897–1912.
 22. Choi H, Nesvizhskii AI. False discovery rates and related statistical concepts in mass spectrometry-based proteomics. *J Proteome Res* 2008;7:47–50.
 23. Huang DW, Sherman BT, Lempicki RA. Systematic and integrative analysis of large gene lists using DAVID bioinformatics resources. *Nat Protoc* 2009;4:44–57.
 24. Huang DW, Sherman BT, Lempicki RA. Bioinformatics enrichment tools: paths toward the comprehensive functional analysis of large gene lists. *Nucleic Acids Res* 2009;37:1–13.
 25. Lo Conte M, Carroll KS. The redox biochemistry of protein sulfenylation and sulfinylation. *J Biol Chem* 2013;288:26480–26488.
 26. Leonard SE, Reddie KG, Carroll KS. Mining the thiol proteome for sulfenic acid modifications reveals new targets for oxidation in cells. *ACS Chem Biol* 2009;4:783–799.
 27. Logsdon CD, Ji B. The role of protein synthesis and digestive enzymes in acinar cell injury. *Nat Rev Gastroenterol Hepatol* 2013;10:362–370.
 28. Sah RP, Dudeja V, Dawra RK, Saluja AK. Cerulein-induced chronic pancreatitis does not require intra-acinar activation of trypsinogen in mice. *Gastroenterology* 2013;144:1076–1085 e2.
 29. Schneidenburger J, Weber IA, Hahn D, Buchwalow I, Kruger B, Albrecht E, Domschke W, Lerch MM. The role of kinesin, dynein and microtubules in pancreatic secretion. *Cell Mol Life Sci* 2009;66:2525–2537.
 30. Shannon P, Markiel A, Ozier O, Baliga NS, Wang JT, Ramage D, Amin N, Schwikowski B, Ideker T. Cytoscape: a software environment for integrated models of biomolecular interaction networks. *Genome Res* 2003;13:2498–2504.
 31. Vonlaufen A, Wilson JS, Pirola RC, Apte MV. Role of alcohol metabolism in chronic pancreatitis. *Alcohol Res Health* 2007;30:48–54.
 32. Johansson BB, Torsvik J, Bjorkhaug L, Vesterhus M, Ragvin A, Tjora E, Fjeld K, Hoem D, Johansson S, Raeder H, Lindquist S, Hernell O, Cnop M, Saraste J, Flatmark T, Molven A, Njolstad PR. Diabetes and pancreatic exocrine dysfunction due to mutations in the carboxyl ester lipase gene-maturity onset diabetes of the young (CEL-MODY): a protein misfolding disease. *J Biol Chem* 2011;286:34593–34605.
 33. Huang W, Booth DM, Cane MC, Chvanov M, Javed MA, Elliott VL, Armstrong JA, Dingsdale H, Cash N, Li Y, Greenhalf W, Mukherjee R, Kaphalia BS, Jaffar M, Petersen OH, Tepikin AV, Sutton R, Criddle DN. Fatty acid ethyl ester synthase inhibition ameliorates ethanol-induced Ca²⁺-dependent mitochondrial dysfunction and acute pancreatitis. *Gut* 2014;63:1313–1324.
 34. Ron D, Walter P. Signal integration in the endoplasmic reticulum unfolded protein response. *Nat Rev Mol Cell Biol* 2007;8:519–529.
 35. Colicelli J. Human RAS superfamily proteins and related GTPases. *Sci STKE* 2004;2004:RE13.
 36. Ohnishi H, Samuelson LC, Yule DI, Ernst SA, Williams JA. Overexpression of Rab3D enhances regulated amylase secretion from pancreatic acini of transgenic mice. *J Clin Invest* 1997;100:3044–3052.
 37. Riedel D, Antonin W, Fernandez-Chacon R, Alvarez de Toledo G, Jo T, Geppert M, Valentijn JA, Valentijn K, Jamieson JD, Sudhof TC, Jahn R. Rab3D is not required for exocrine exocytosis but for maintenance of normally sized secretory granules. *Mol Cell Biol* 2002;22:6487–6497.
 38. Galea G, Bexiga MG, Panarella A, O'Neill ED, Simpson JC. A high-content screening microscopy approach to dissect the role of Rab proteins in Golgi-

- to-ER retrograde trafficking. *J Cell Sci* 2015; 128:2339–2349.
39. Gao X, Fu X, Song J, Zhang Y, Cui X, Su C, Ge L, Shao J, Xin L, Saarikettu J, Mei M, Yang X, Wei M, Silvennoinen O, Yao Z, He J, Yang J. Poly(A)(+) mRNA-binding protein Tudor-SN regulates stress granules aggregation dynamics. *FEBS J* 2015;282:874–890.
 40. Fratelli M, Demol H, Puype M, Casagrande S, Villa P, Eberini I, Vandekerckhove J, Gianazza E, Ghezzi P. Identification of proteins undergoing glutathionylation in oxidatively stressed hepatocytes and hepatoma cells. *Proteomics* 2003;3:1154–1161.
 41. Lind C, Gerdes R, Hamnell Y, Schuppe-Koistinen I, von Lowenhilf HB, Holmgren A, Cotgreave IA. Identification of S-glutathionylated cellular proteins during oxidative stress and constitutive metabolism by affinity purification and proteomic analysis. *Arch Biochem Biophys* 2002; 406:229–240.
 42. Petrushanko IY, Yakushev S, Mitkevich VA, Kamanina YV, Ziganshin RH, Meng X, Anashkina AA, Makhro A, Lopina OD, Gassmann M, Makarov AA, Bogdanova A. S-glutathionylation of the Na, K-ATPase catalytic alpha subunit is a determinant of the enzyme redox sensitivity. *J Biol Chem* 2012;287:32195–32205.
 43. Ye ZW, Zhang J, Ancrum T, Manevich Y, Townsend DM, Tew KD. Glutathione S-transferase p-mediated protein s-glutathionylation of resident endoplasmic reticulum proteins influences sensitivity to drug-induced unfolded protein response. *Antioxid Redox Signal* 2017;26:247–261.
 44. Galligan JJ, Smathers RL, Shearn CT, Fritz KS, Backos DS, Jiang H, Franklin CC, Orlicky DJ, Maclean KN, Petersen DR. Oxidative stress and the ER stress response in a murine model for early-stage alcoholic liver disease. *J Toxicol* 2012;2012:207594.
 45. McGarry DJ, Chen W, Chakravarty P, Lamont DL, Wolf CR, Henderson CJ. Proteome-wide identification and quantification of S-glutathionylation targets in mouse liver. *Biochem J* 2015;469:25–32.
 46. Criddle DN. The role of fat and alcohol in acute pancreatitis: a dangerous liaison. *Pancreatology* 2015; 15(Suppl):S6–S12.
 47. Vakos HT, Burton GW, Kaplan H. Taurocholate-induced dimerization of bovine cholesterol esterase in sodium dodecylsulfate. *Biochim Biophys Acta* 1997; 1342:103–108.
 48. Wang X, Wang CS, Tang J, Dyda F, Zhang XC. The crystal structure of bovine bile salt activated lipase: insights into the bile salt activation mechanism. *Structure* 1997;5:1209–1218.
 49. Torsvik J, Johansson BB, Dalva M, Marie M, Fjeld K, Johansson S, Bjorkoy G, Saraste J, Njolstad PR, Molven A. Endocytosis of secreted carboxyl ester lipase in a syndrome of diabetes and pancreatic exocrine dysfunction. *J Biol Chem* 2014;289:29097–29111.
 50. Yoshida H, Matsui T, Hosokawa N, Kaufman RJ, Nagata K, Mori K. A time-dependent phase shift in the mammalian unfolded protein response. *Dev Cell* 2003; 4:265–271.
 51. Hartley CL, Edwards S, Mullan L, Bell PA, Fresquet M, Boot-Handford RP, Briggs MD. Armet/Manf and Creld2 are components of a specialized ER stress response provoked by inappropriate formation of disulphide bonds: implications for genetic skeletal diseases. *Hum Mol Genet* 2013;22:5262–5275.
 52. Yang J, Bennett BD, Luo S, Inoue K, Grimm SA, Schroth GP, Bushel PR, Kinyamu HK, Archer TK. LIN28A modulates splicing and gene expression programs in breast cancer cells. *Mol Cell Biol* 2015; 35:3225–3243.
 53. Meunier L, Usherwood YK, Chung KT, Hendershot LM. A subset of chaperones and folding enzymes form multiprotein complexes in endoplasmic reticulum to bind nascent proteins. *Mol Biol Cell* 2002; 13:4456–4469.
 54. Behnke J, Feige MJ, Hendershot LM. BiP and its nucleotide exchange factors Grp170 and Sil1: mechanisms of action and biological functions. *J Mol Biol* 2015; 427:1589–1608.
 55. Smith AJ, Daut J, Schwappach B. Membrane proteins as 14-3-3 clients in functional regulation and intracellular transport. *Physiology (Bethesda)* 2011;26:181–191.
 56. Bajaj Pahuja K, Wang J, Blagoveshchenskaya A, Lim L, Madhusudhan MS, Mayinger P, Schekman R. Phosphoregulatory protein 14-3-3 facilitates SAC1 transport from the endoplasmic reticulum. *Proc Natl Acad Sci U S A* 2015;112:E3199–E3206.
 57. Meek SE, Lane WS, Piwnicka-Worms H. Comprehensive proteomic analysis of interphase and mitotic 14-3-3-binding proteins. *J Biol Chem* 2004;279:32046–32054.
 58. Dubois F, Vandermoere F, Gernez A, Murphy J, Toth R, Chen S, Geraghty KM, Morrice NA, MacKintosh C. Differential 14-3-3 affinity capture reveals new downstream targets of phosphatidylinositol 3-kinase signaling. *Mol Cell Proteomics* 2009;8:2487–2499.
 59. Pandol SJ, Periskic S, Gukovsky I, Zaninovic V, Jung Y, Zong Y, Solomon TE, Gukovskaya AS, Tsukamoto H. Ethanol diet increases the sensitivity of rats to pancreatitis induced by cholecystokinin octapeptide. *Gastroenterology* 1999;117:706–716.
 60. Lam PP, Cosen Binker LI, Lugea A, Pandol SJ, Gaisano HY. Alcohol redirects CCK-mediated apical exocytosis to the acinar basolateral membrane in alcoholic pancreatitis. *Traffic* 2007;8:605–617.
 61. Kubisch CH, Gukovsky I, Lugea A, Pandol SJ, Kuick R, Misek DE, Hanash SM, Logsdon CD. Long-term ethanol consumption alters pancreatic gene expression in rats: a possible connection to pancreatic injury. *Pancreas* 2006; 33:68–76.
 62. Lugea A, Gukovsky I, Gukovskaya AS, Pandol SJ. Non-oxidative ethanol metabolites alter extracellular matrix protein content in rat pancreas. *Gastroenterology* 2003; 125:1845–1859.
 63. Setiawan VW, Pandol SJ, Porcel J, Wilkens LR, Le Marchand L, Pike MC, Monroe KR. Prospective study of alcohol drinking, smoking, and pancreatitis: the Multi-ethnic Cohort. *Pancreas* 2016;45:819–825.
 64. Setiawan VW, Monroe KR, Lugea A, Yadav D, Pandol SJ. Uniting epidemiology and experimental disease models for alcohol-related pancreatic disease. *Alcohol Res* 2017; 38:1–10.

65. Eletto D, Chevet E, Argon Y, Appenzeller-Herzog C. Redox controls UPR to control redox. *J Cell Sci* 2014; 127:3649–3658.

Received July 8, 2017. Accepted January 2, 2018.

Correspondence

Address correspondence to: Richard T. Waldron, PhD, Department of Medicine, Cedars-Sinai Medical Center, 8700 Beverly Boulevard, Davis Building, D3096, Los Angeles, California 90048. e-mail: Richard.Waldron@cshs.org; fax: (310) 423-3184.

Acknowledgments

The authors thank Hide Tsukamoto and the Southern California Center for Alcoholic Liver and Pancreas Diseases and Cirrhosis for mouse ethanol feeding; Laurie Glimcher for *Xbp1*^{+/-} mice; the Cedars-Sinai Medical Center Biomarker Discovery Core for mass spectrometry services; the Veteran's Administration Greater Los Angeles Healthcare System confocal microscopy

Core for support with imaging analysis; and Christopher Holland for assistance with microscopic imaging.

Author contributions

Richard T. Waldron and Aurelia Lugea designed, conducted, and interpreted experiments, and wrote the paper; Hsin-Yuan Su assisted with the animal model and protein analysis; Honit Piplani assisted with network analysis; Joseph Capri, Whitaker Cohn, Julian P. Whitelegge, Wei Yang, Bo Zhou, Kym F. Faull, and Michael R. Freeman performed mass spectrometry and analyzed data with Richard T. Waldron; Sugunadevi Sakkiah and Ravinder Abrol performed structural modeling computation; and Stephen J. Pandol assisted Richard T. Waldron and Aurelia Lugea with the project design and data interpretation.

Conflicts of interest

The authors disclose no conflicts.

Funding

Supported by National Institute of Health grants R01 AA019954 (A.L.), P01DK098108, P01CA163200, and P50AA11999 (S.J.P.).